Searches for Higgs boson pair production with the full LHC Run 2 dataset in ATLAS

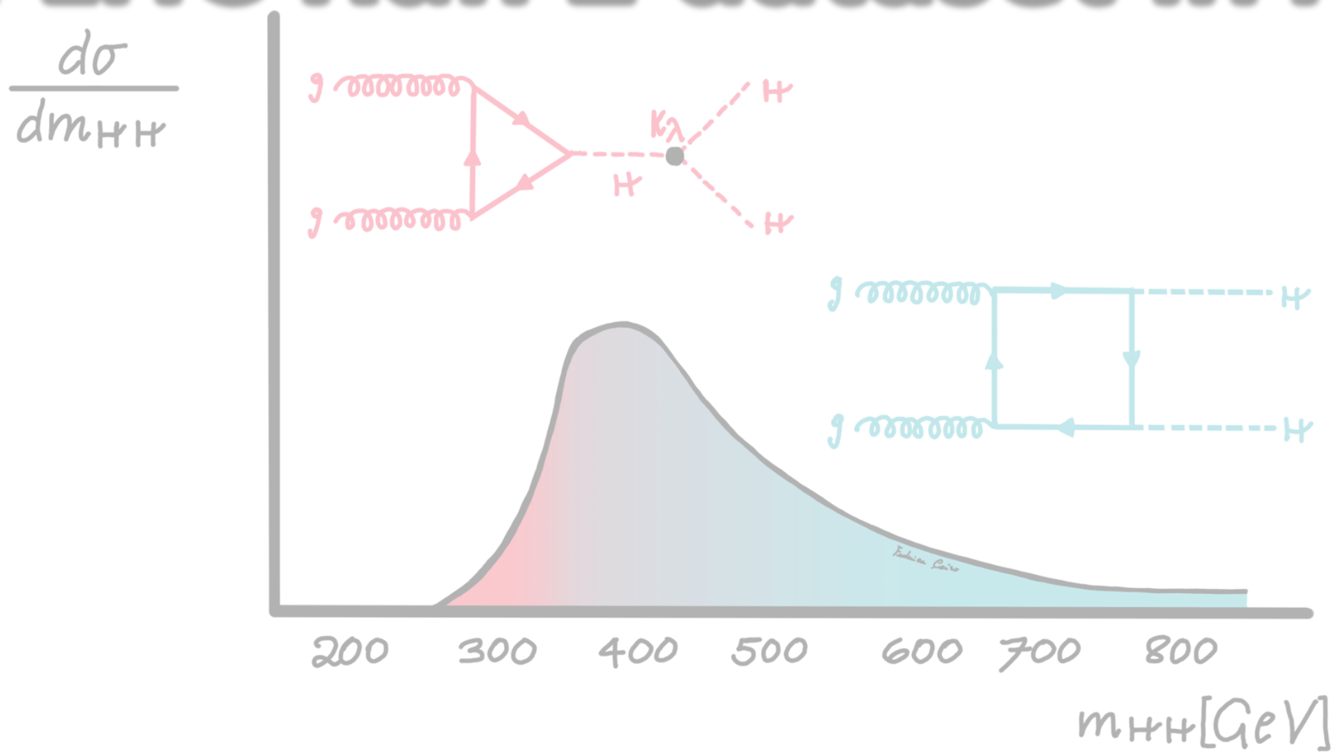

EPS-HEP Conference 2021

Valentina Maria Martina Cairo

SLAC NATIONAL ACCELERATOR LABORATORY

Physics Motivation

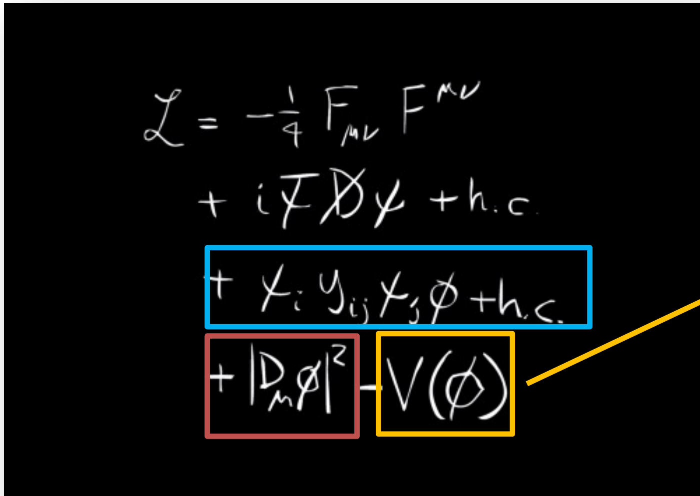

$$V(\phi^\dagger \phi) = \mu^2 \phi^\dagger \phi + \lambda (\phi^\dagger \phi)^2$$
$$\supset \lambda v^2 H^2 + \lambda v H^3 + \frac{\lambda}{4} H^4$$

$$m_H = \sqrt{2\lambda v^2}$$
$$v \simeq 246 \text{ GeV}$$
$$\kappa_\lambda = \lambda_{HHH} / \lambda_{SM}$$

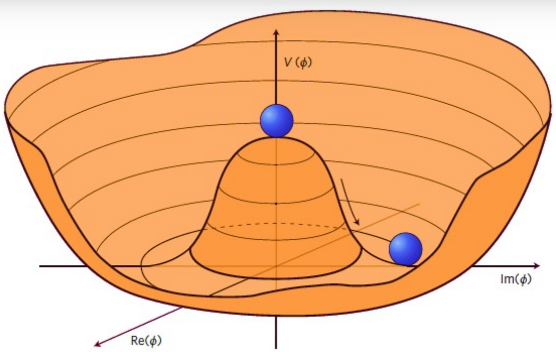

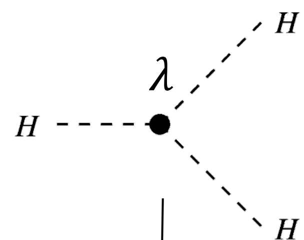

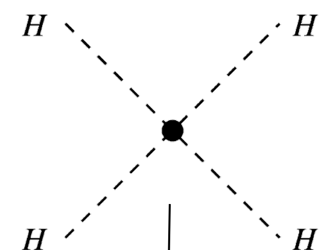

Direct access to λ in HH pair production

Out of reach even for HL-LHC

Known m_H (~125 GeV), SM predicts λ (~0.13)

New physics can alter this number

→ Implications on the stability of the Universe

Probing the **Higgs-self coupling** is a **key goal for HL-LHC**, but much can be done now!

HH Production at the LHC

Non-resonant σ_{HH}^{ggF} = 31.05 fb at 13 TeV for m_H = 125.00 GeV

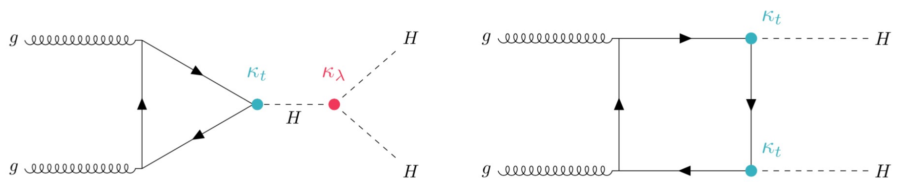

Non-resonant σ_{HH}^{VBF} = 1.73 fb at 13 TeV for m_H = 125.00 GeV

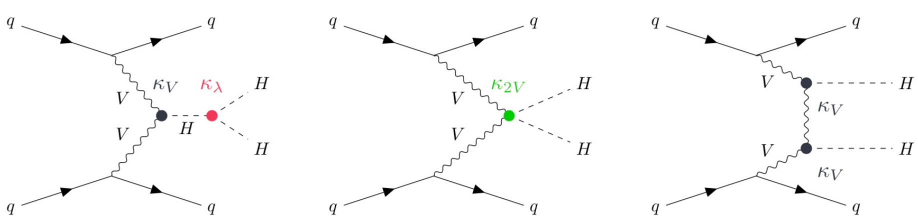

Resonant ggF

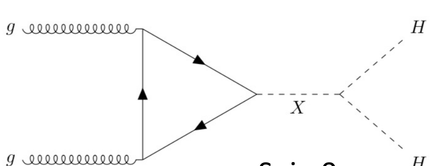

Spin 0

Spin 2

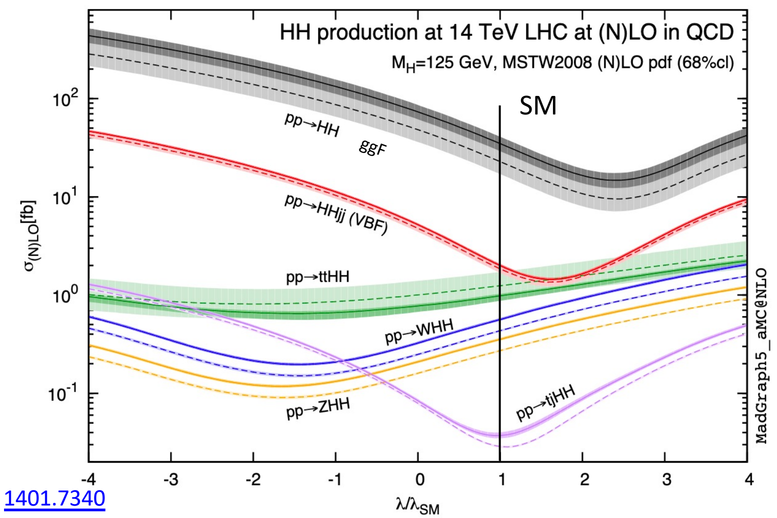

1401.7340

σ_{HH} and **kinematics** depend on the **couplings** and presence of new **resonances**

New physics can manifest as deviation in σ_{HH}

HH Final States

σ_{HH} @ 13 TeV ~ **30 fb**
(1000 x smaller than single H)

Run 2 $\int L \sim$ **140 fb^{-1}**

~ **4k HH** events

Scales up to about
10^5 in HL-LHC

Combination
(and complementarity)
of various final states
fundamental for observation!

Most final states rely on
b-tagging

Branching Ratio	bb	WW	ττ	ZZ	γγ
bb	33%				
WW	25%	4.6%			
ττ	7.4%	2.5%	0.39%		
ZZ	3.1%	1.2%	0.34%	0.076%	
γγ	0.26%	0.10%	0.029%	0.013%	0.0005%

Most recent full Run 2 ATLAS Results covered today:
$HH \rightarrow b\bar{b}\gamma\gamma$ (resonant & non-resonant)
$HH \rightarrow b\bar{b}\tau\tau$ (resonant & non-resonant)
$HH \rightarrow b\bar{b}b\bar{b}$ (resonant)

$HH \to b\bar{b}\gamma\gamma$

Please check out also
M. Belfkir's
and
R. Hulsken's
posters!

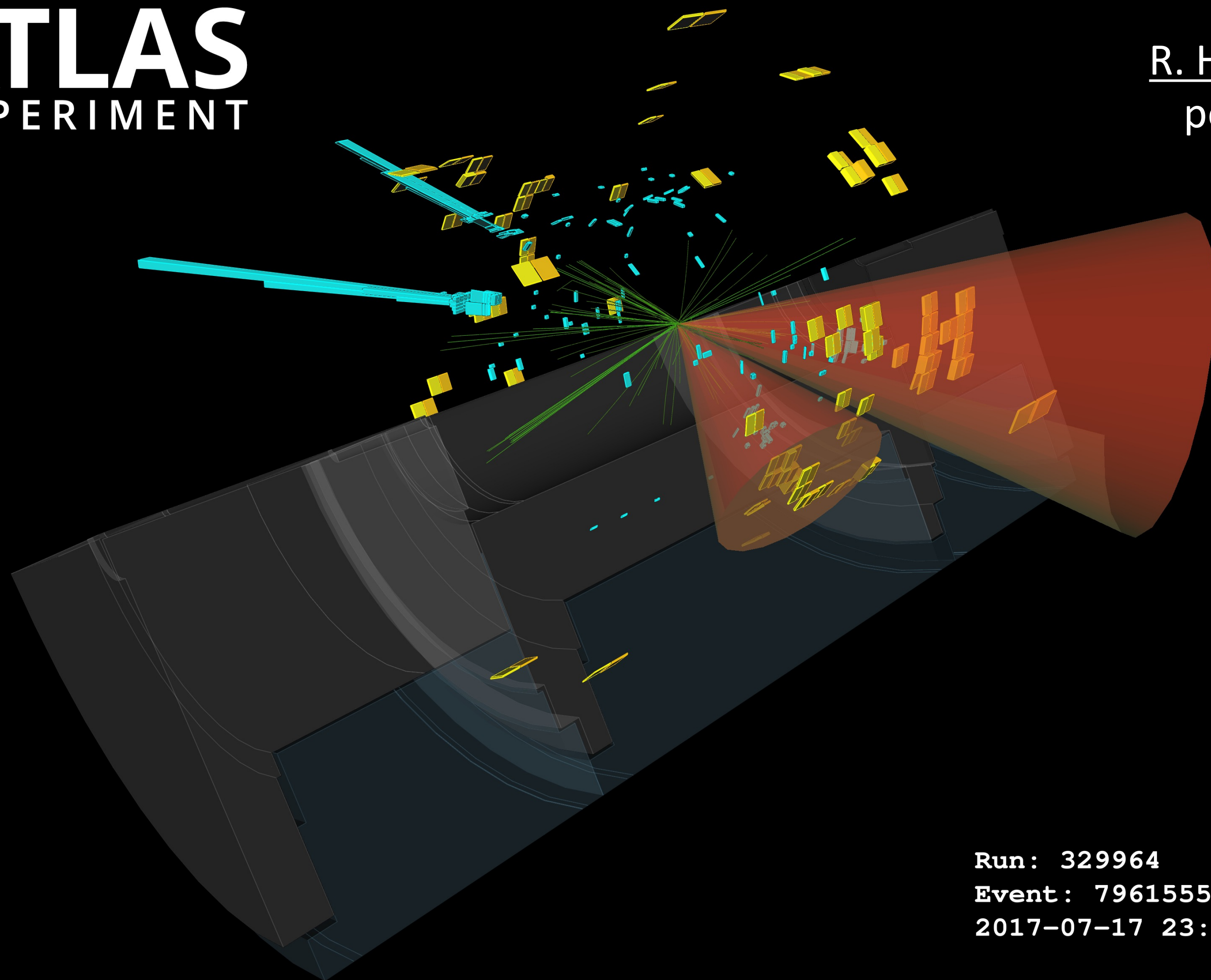

Run: 329964
Event: 796155578
2017-07-17 23:58:15 CEST

Publication: ATLAS-CONF-2021-016
Physics Briefing: https://atlas.cern/updates/briefing/twice-higgs-twice-challenge

$HH \to b\bar{b}\gamma\gamma$ analysis in a nutshell

Small BR, but fully **reconstructable** final state, **clean signal extraction**

Di-photon triggers with **E_T > 35, 25 GeV** (82.9% efficiency for non-resonant signal, 69.5% for m_X = 300 GeV)

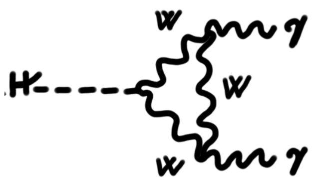

Tight and isolated

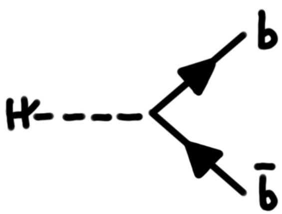

B-jet energy corrections

Object selection

Event categorization

MVA approach

4 categories for non-resonant analysis

1 category per m_X for resonant analysis

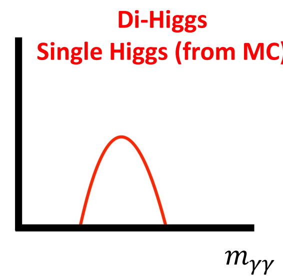

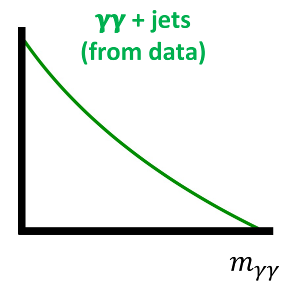

Modeling of discriminant variable

Simultaneous likelihood fit to all categories

SM $\boldsymbol{\sigma}$ limits and

$\boldsymbol{\sigma}$ **vs** $\boldsymbol{k_\lambda}$

for **non resonant** analysis

$\boldsymbol{\sigma}$ **vs** $\boldsymbol{m_X}$

for **resonant** analysis

Non-Resonant $HH \to b\bar{b}\gamma\gamma$

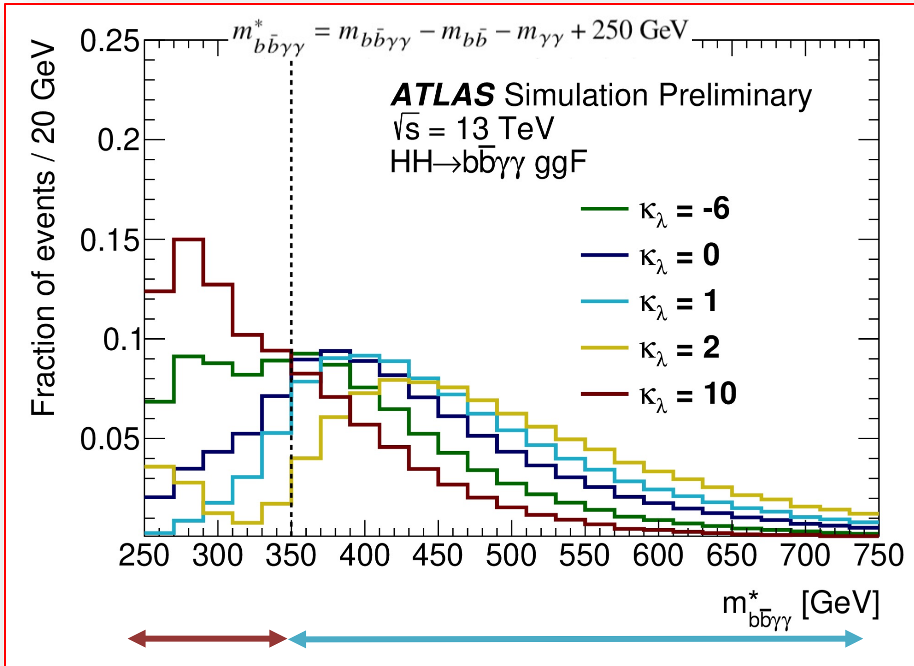

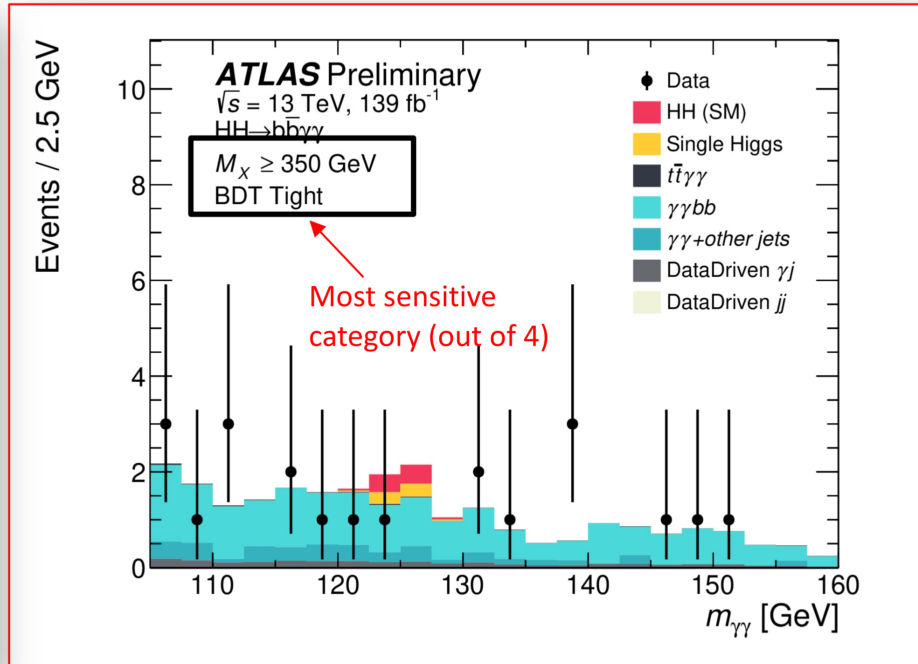

- **Low** and **High** $m^*_{b\bar{b}\gamma\gamma}$
  - **< 350 GeV for BSM**, **> 350 GeV for SM**
- BDT to discriminate signal ($k_\lambda = 1, 10$) from backgrounds
  - m_{bb} very powerful (b-jet energy corrections improve resolution by ~ **20%**)
- **Loose** and **Tight BDT**
  - Boundaries chosen to maximize combined expected significance

Non-Resonant $HH \rightarrow b\bar{b}\gamma\gamma$ results

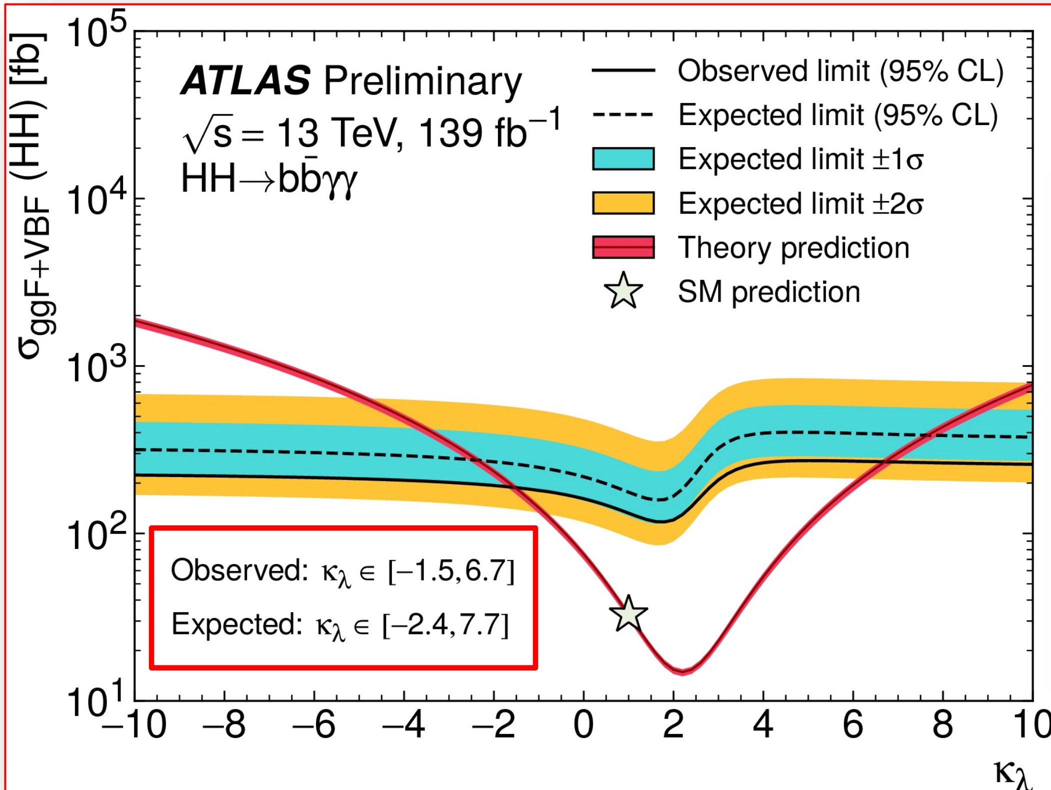

Earlier ATLAS results

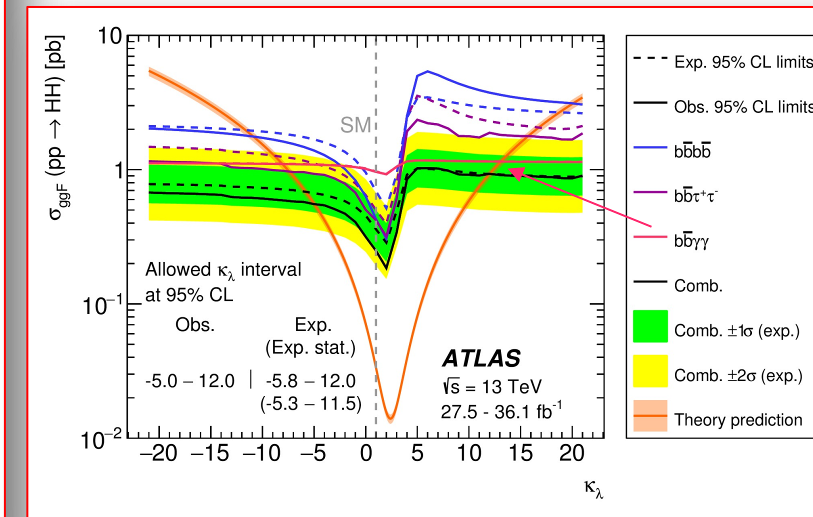

4.1 (5.5) x SM σ_{HH}

5x improvement wrt previous result (~ 26 x SM), ~3x due to analysis techniques

driven by m_{HH} categorization & MVA as well as b-jet corrections

Statistically dominated, few % impact from systematics

World's best constraints to date on Higgs boson's self coupling!

Resonant $HH \rightarrow b\bar{b}\gamma\gamma$ results

- **Single BDT for all resonances (mass dependent cut), 2 BDTs** to separate signal vs **continuum** and **single Higgs** backgrounds, scores combined in BDT_{tot}, signal extracted from $m_{\gamma\gamma}$

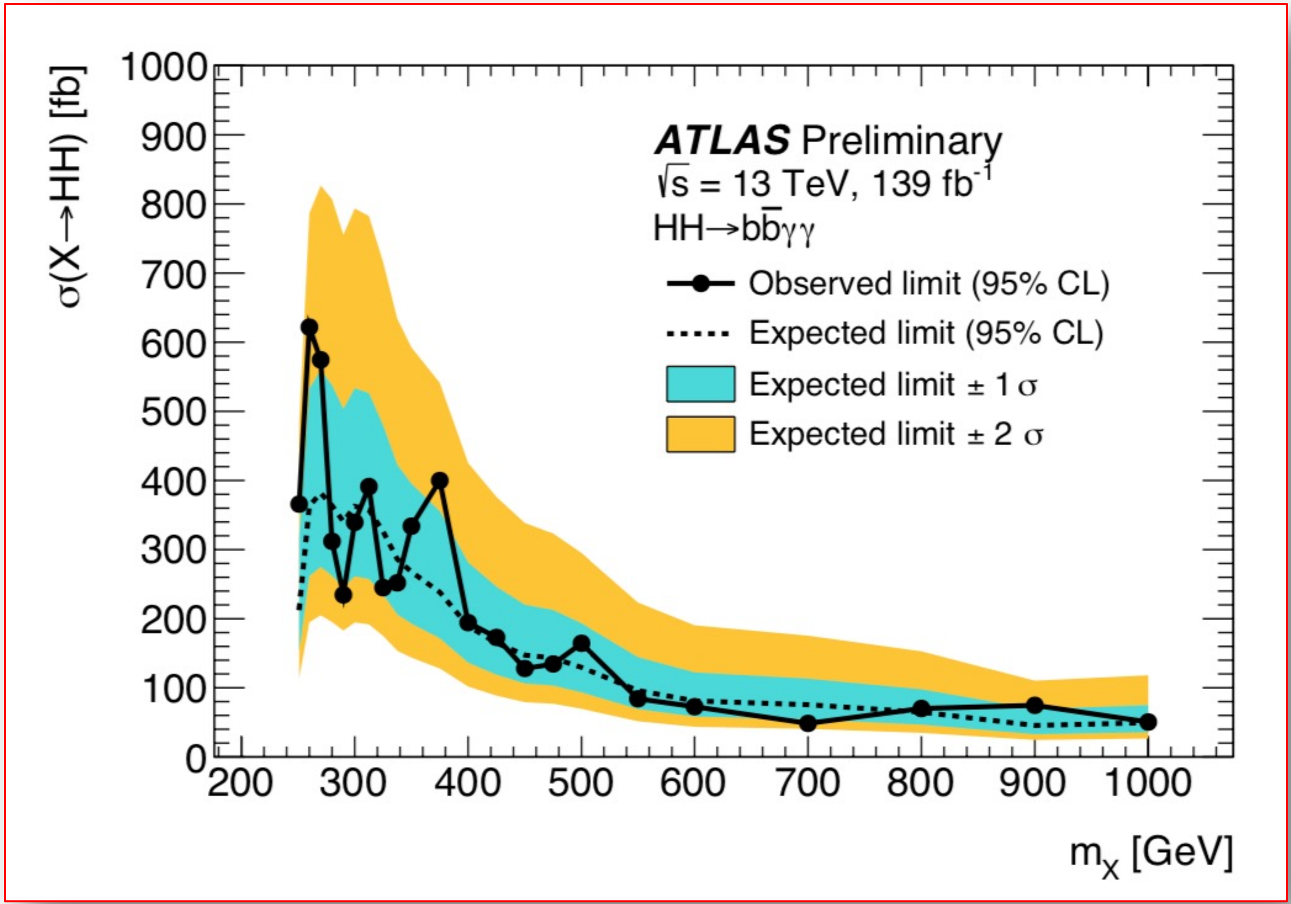

~ 30% improvement from BDT strategy on top of luminosity increase wrt 36 fb^{-1} <u>results</u>

$HH \to b\bar{b}\tau\tau$

$\tau_{had} - \tau_{had}$

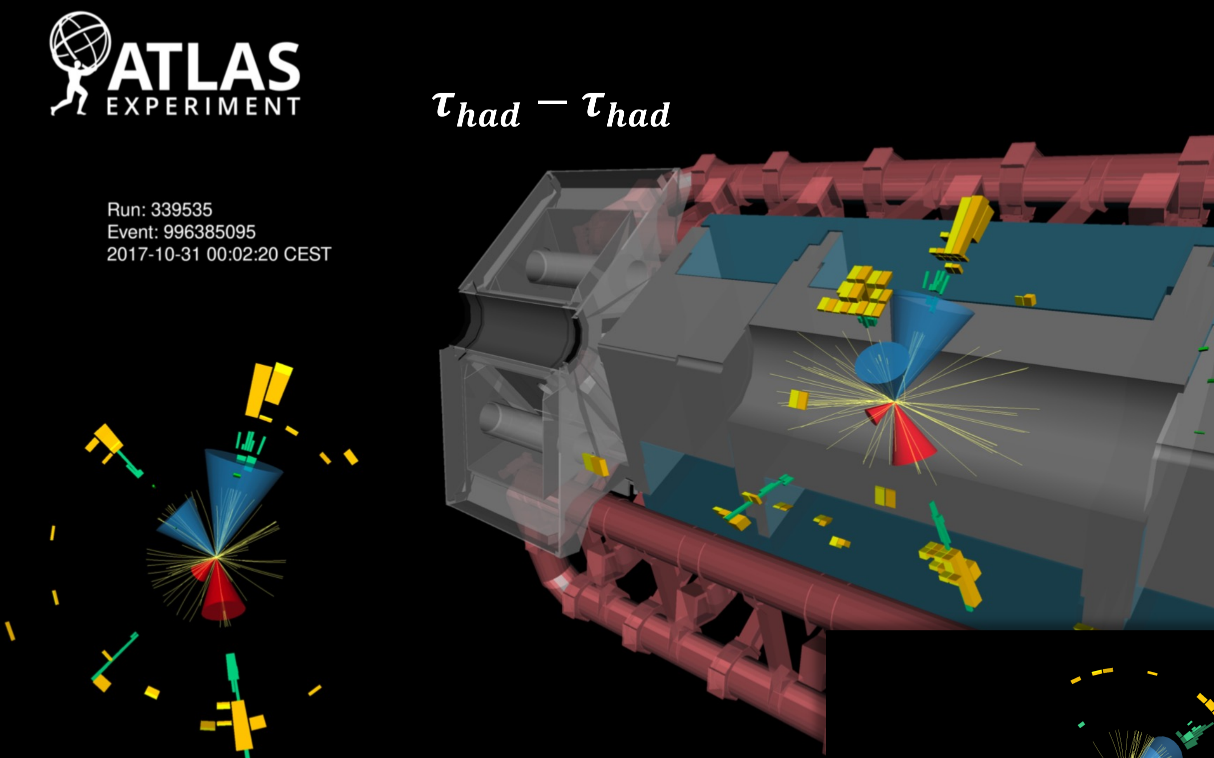

$\tau_{lep} - \tau_{had}$

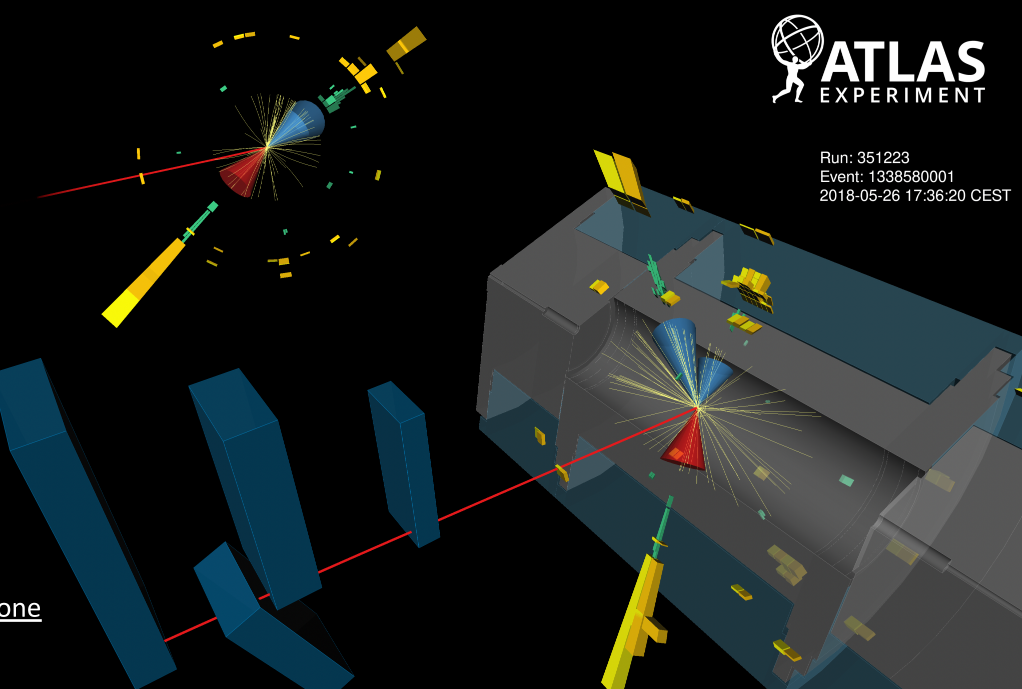

Publication: [ATLAS-CONF-2021-030]

Physics Briefing: [https://atlas.cern/updates/briefing/two-Higgs-better-one]

$HH \to b\bar{b}\tau\tau$ analysis (1)

Relatively large BR and **relatively clean final state**

Single Tau Trigger & **Di-Tau** Trigger **for $\tau_{had}\,\tau_{had}$**

Single Lepton Trigger (SLT) and **Lepton+Tau Trigger** (LTT) **in $\tau_{lep}\,\tau_{had}$**

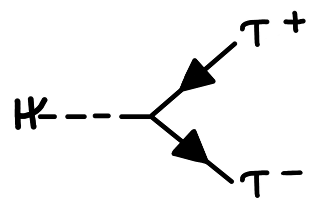

Hadronic & Leptonic

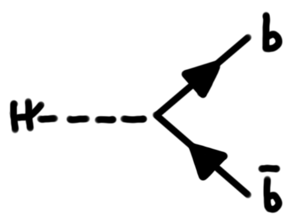

B-jet energy corrections

Object selection

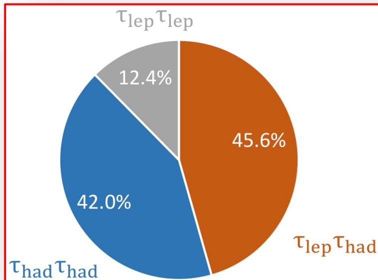

Event categorization

MVA in 3 categories:

$\tau_{had}\,\tau_{had}$
(opp. charged)

$\tau_{lep}\,\tau_{had}$ (e/μ & opp. charged τ) **LTT** **SLT**

Control region for Z+HF (m_{ll})

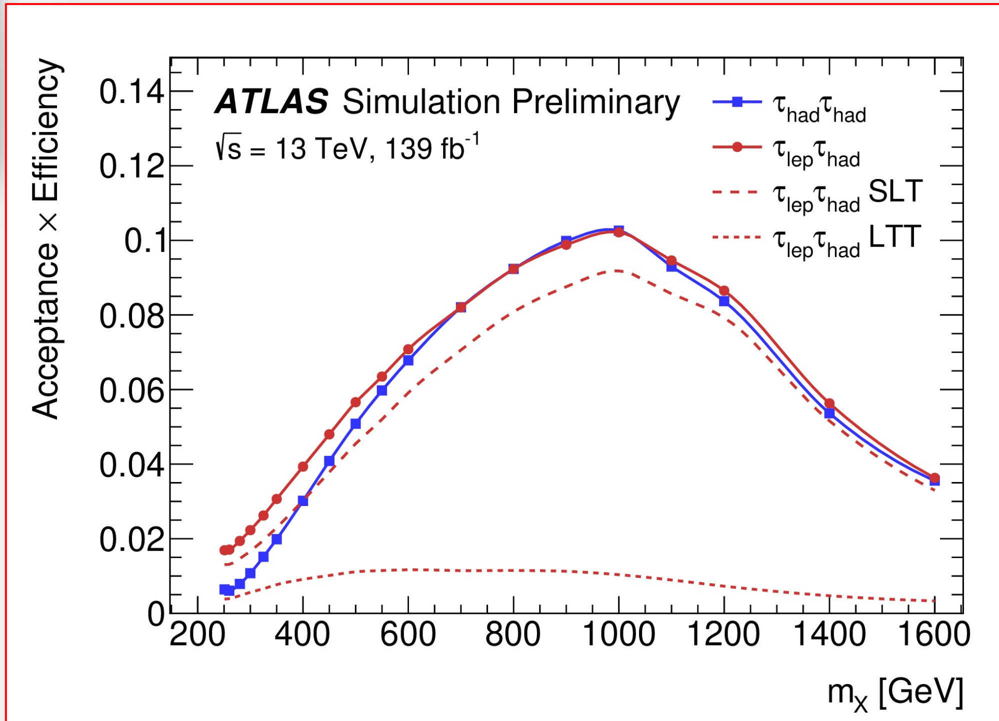

$HH \rightarrow b\bar{b}\tau\tau$ analysis (2)

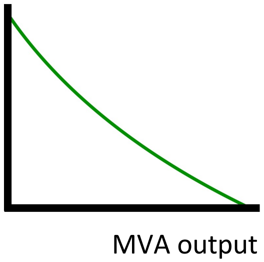

Parametric (by m_X) NNs for resonant

BDT($\tau_{had}\,\tau_{had}$) & NN($\tau_{lep}\,\tau_{had}$) for non-resonant

m_{HH}, m_{bb}, $m_{\tau\tau}$, etc.

Multi-variable signal extraction

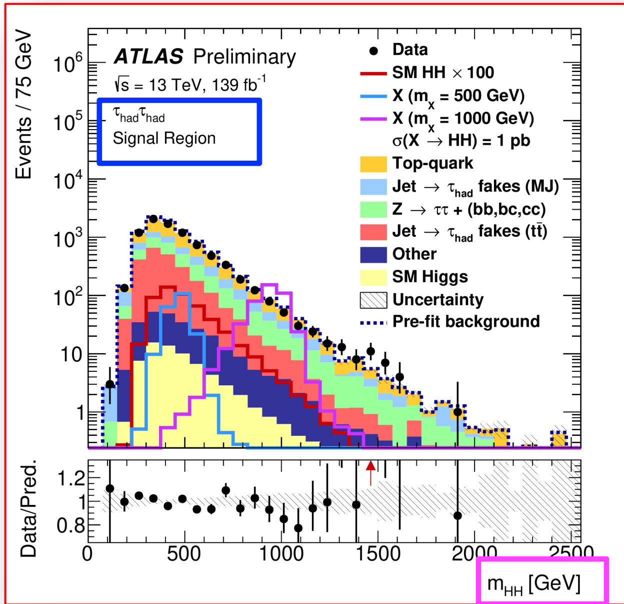

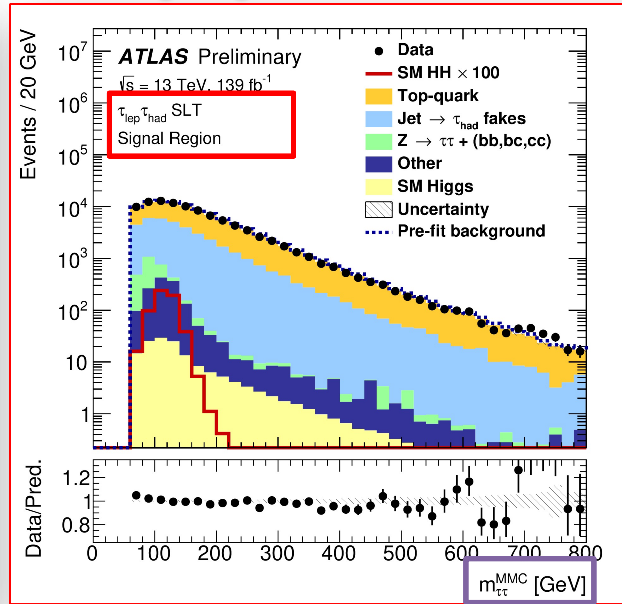

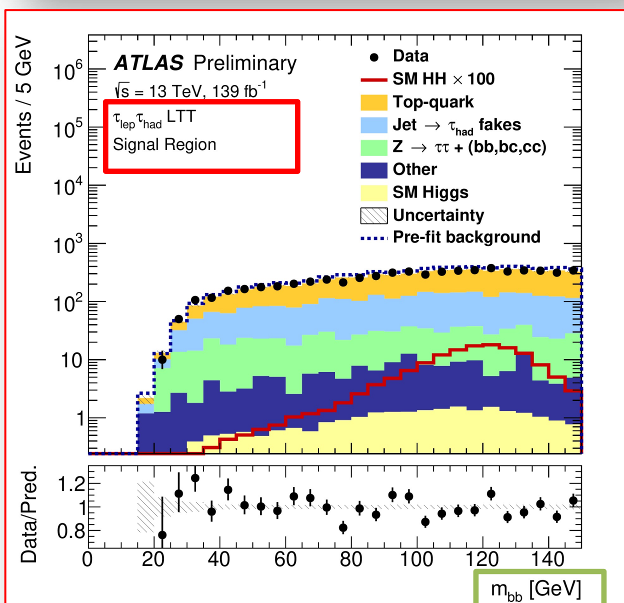

Backgrounds from:

true τ in $t\bar{t}$ and **Z+HF** (from MC, normalization from data)

fake τ in $t\bar{t}$ and **multi-jet** (data-driven)

Non-resonant $HH \rightarrow b\bar{b}\tau\tau$ results

Binned maximum-likelihood fit of the MVA score to data
(simultaneous in all categories)

Non-resonant analysis thoroughly optimized for SM cross-section limit!

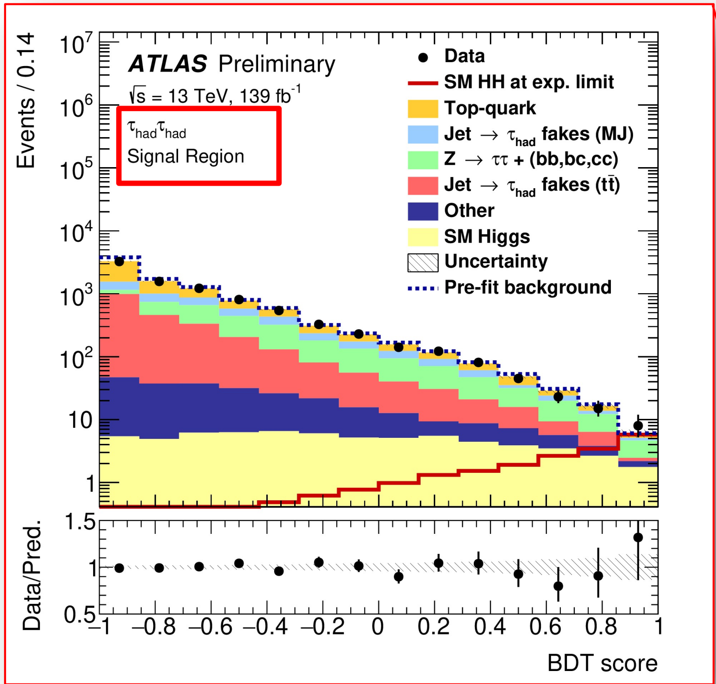

		Observed	$-2\ \sigma$	$-1\ \sigma$	Expected	$+1\ \sigma$	$+2\ \sigma$
$\tau_{\text{had}}\tau_{\text{had}}$	$\sigma_{\text{ggF+VBF}}$ [fb]	145	70.5	94.6	131	183	245
	$\sigma_{\text{ggF+VBF}}/\sigma^{\text{SM}}_{\text{ggF+VBF}}$	4.95	2.38	3.19	4.43	6.17	8.27
$\tau_{\text{lep}}\tau_{\text{had}}$	$\sigma_{\text{ggF+VBF}}$ [fb]	265	124	167	231	322	432
	$\sigma_{\text{ggF+VBF}}/\sigma^{\text{SM}}_{\text{ggF+VBF}}$	9.16	4.22	5.66	7.86	10.9	14.7
Combined	$\sigma_{\text{ggF+VBF}}$ [fb]	135	61.3	82.3	114	159	213
	$\sigma_{\text{ggF+VBF}}/\sigma^{\text{SM}}_{\text{ggF+VBF}}$	4.65	2.08	2.79	3.87	5.39	7.22

4x improvement wrt to previous results! (12.7 x SM),

2x due to the τ and *b*-jet reconstruction and identification improvements and to analysis techniques (MVA & fake-τ estimation methods).

- Statistically dominated, largest systematics from background modeling

Resonant $HH \rightarrow b\bar{b}\tau\tau$ results

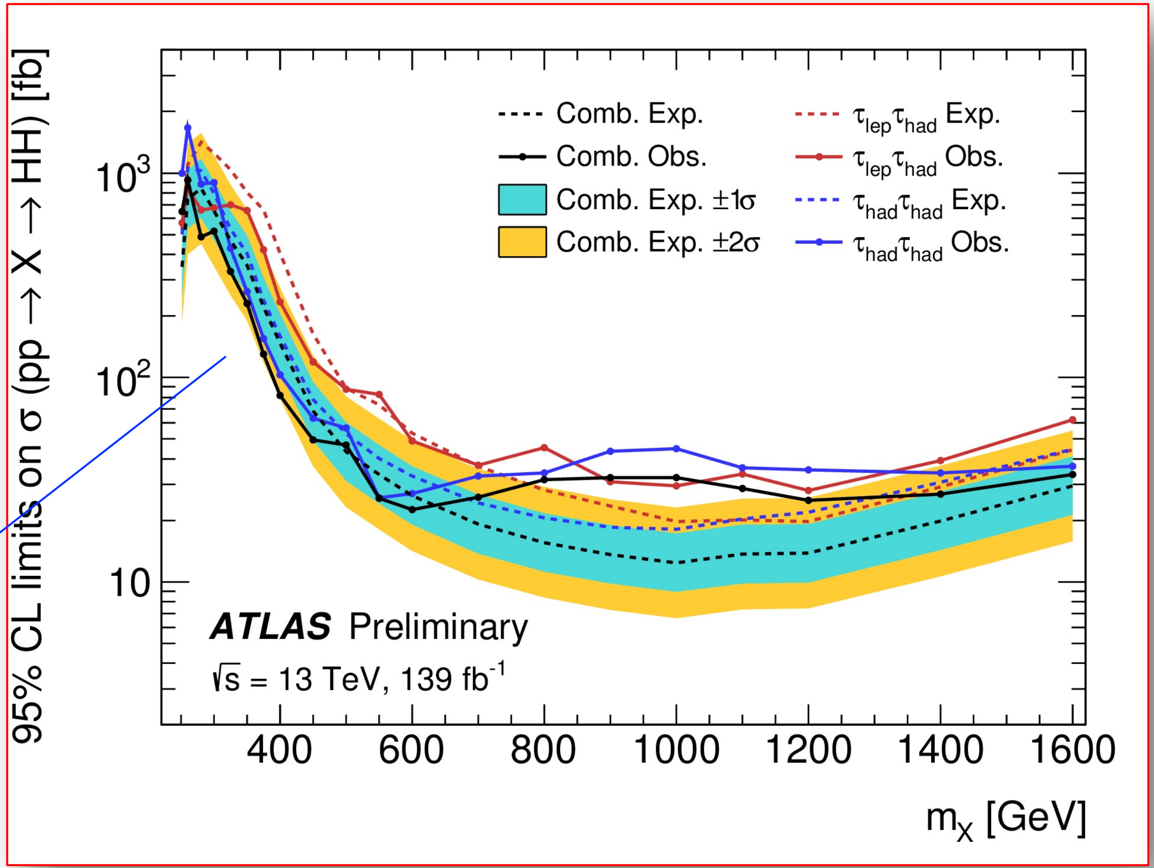

$\tau_{had}\ \tau_{had}$

Better sensitivity below 1 TeV

- Broad excess @ 700 GeV < m_X < 1.2 TeV.
- Most significant excess for $\tau_{had}\ \tau_{had}$ ($\tau_{lep}\ \tau_{had}$) found @ 1 TeV (1.1 TeV), local significance of 2.8 σ (1.6 σ).
- Combined: @1 TeV, local significance 3.1 σ, global significance of $2.1^{+0.4}_{-0.2}\ \sigma$.

$HH \rightarrow b\bar{b}b\bar{b}$

ATLAS EXPERIMENT

Run: 356259
Event: 311347503
2018-07-22 20:00:32 CEST

Boosted

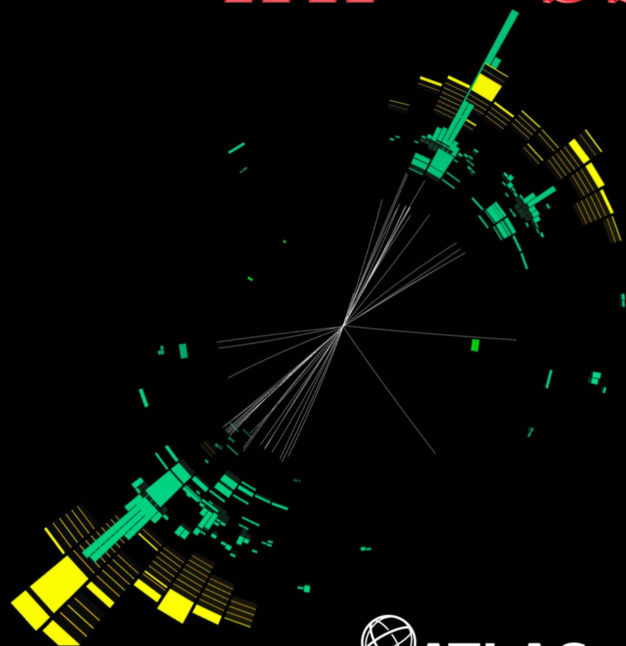

ATLAS EXPERIMENT

Run: 350013
Event: 1556168518
2018-05-11 01:39:26 CEST

Resolved

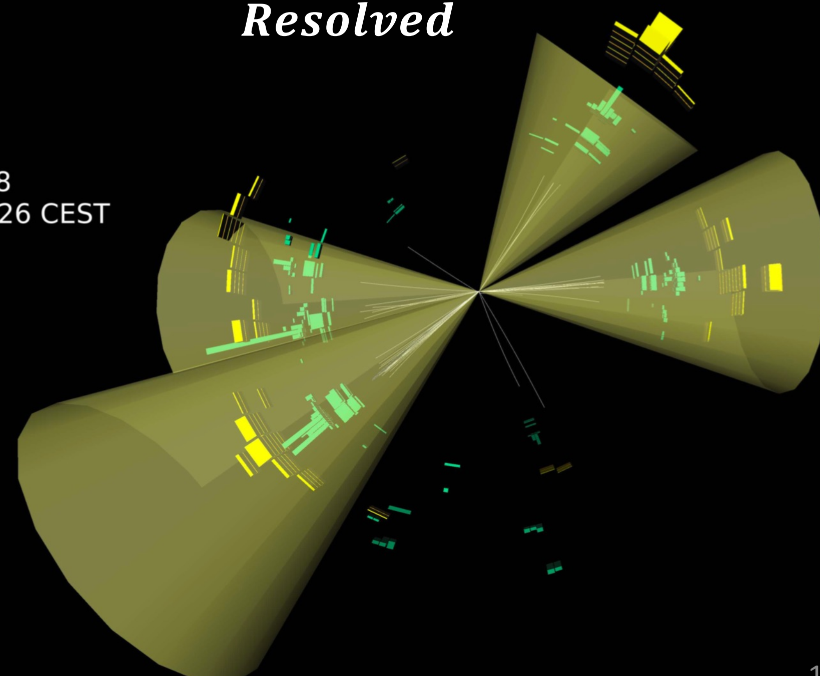

Publication: ATLAS-CONF-2021-035
Physics Briefing: https://atlas.cern/updates/briefing/double-Higgs-to-bottoms

$HH \rightarrow b\bar{b}b\bar{b}$ analysis (1)

Largest BR, but **large multi-jet backgrounds** and challenging combinatorics

Only ggF **resonant** production considered

12 different b-jet & jet triggers for *resolved* (eff up to 80%), single jet trigger for *boosted* (eff ~80%)

Resolved
(251 GeV – 1.5 TeV)
4 b-tagged ΔR=0.4 jets

& Boosted
(900 GeV – 3 TeV)
b-tagged ΔR=1.0 and
VR track-jets

Combined in the overlap region

B-jet energy corrections

Object selection

Event categorization

4b signal region
2b category for bkg estimate

BDT to pair jets from Higgs
(65-100% eff)

Resolved

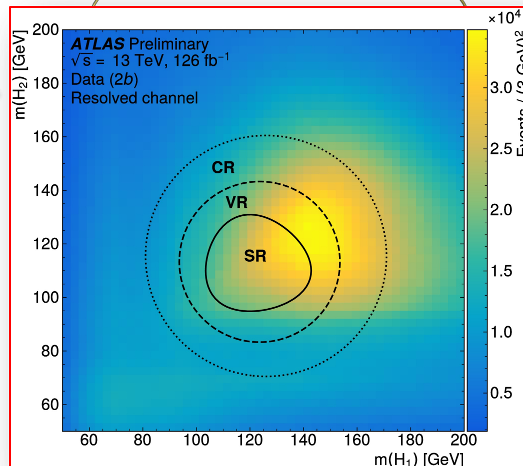

dominated by multi-jet + ~5% $t\bar{t}$

Background modeling

Resolved

Statistical analysis

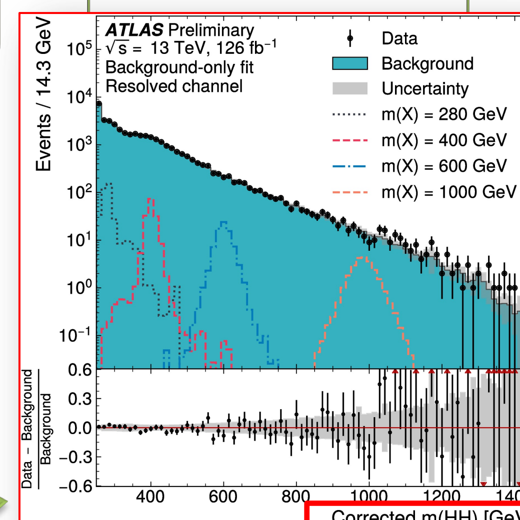

$HH \to b\bar{b}b\bar{b}$ analysis (2)

Largest BR, but **large multi-jet backgrounds** and challenging combinatorics

Only ggF **resonant** production considered

12 different b-jet & jet triggers for *resolved* (eff up to 80%), single jet trigger for *boosted* (eff ~80%)

Resolved
(251 GeV – 1.5 TeV)
4 b-tagged ΔR=0.4 jets

& Boosted
(900 GeV – 3 TeV)
b-tagged ΔR=1.0 and VR track-jets

Combined in the overlap region

B-jet energy corrections

Object selection

Event categorization

signal

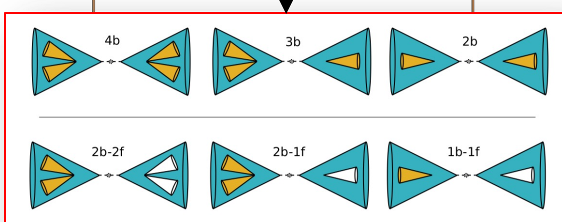

background

CR, VR & SR like in the *resolved* case

Boosted

Bkg dominated by multi-jet + up to 30% $t\bar{t}$

Data-driven multi-jet & MC-driven $t\bar{t}$ (data-driven corrections in 2/3 b region)

Background modeling

Boosted

Statistical Analysis

(3 categories)

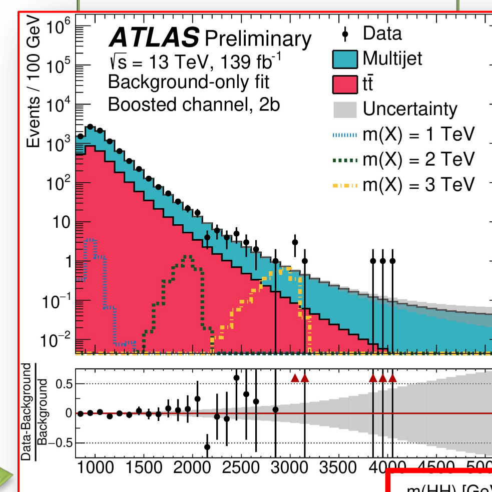

Resonant $HH \to b\bar{b}b\bar{b}$ results

Set upper limits (95% CLs) on cross section times BR(X/G→HH)

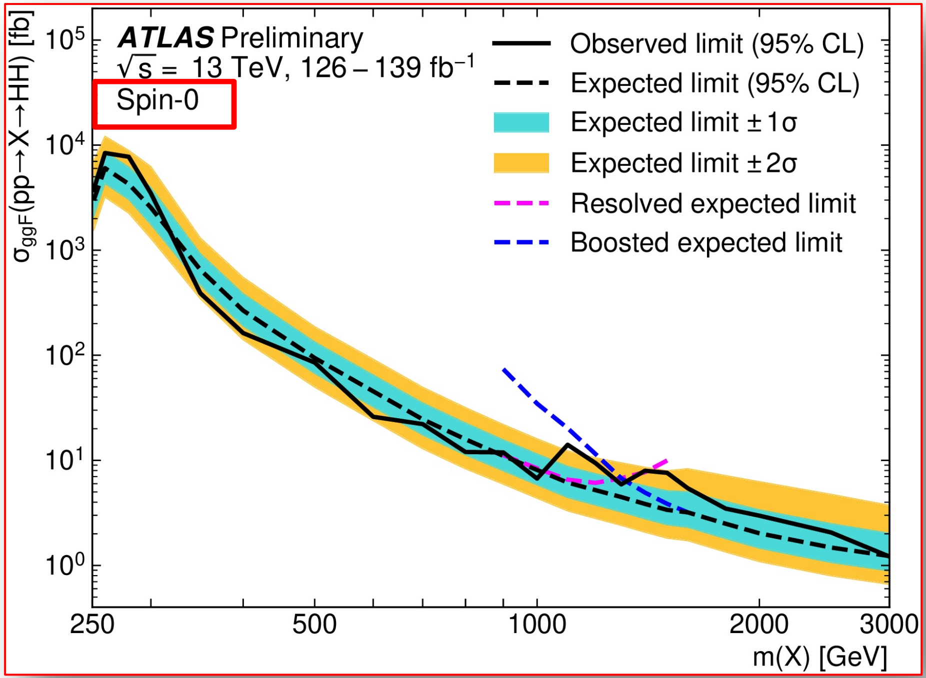

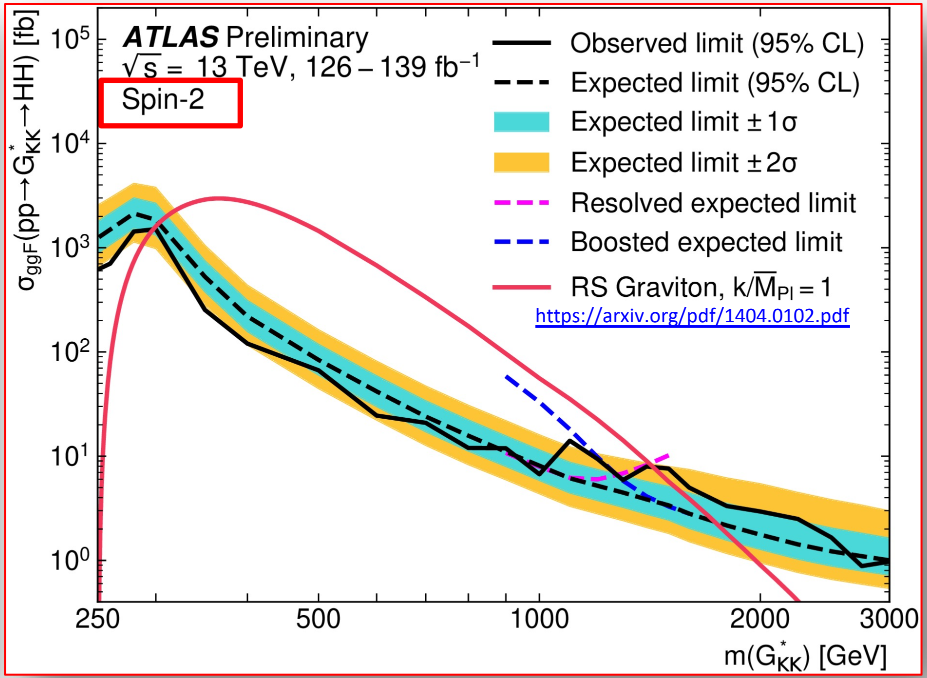

model excluded for graviton masses between 298 GeV and 1440 GeV.

Excess @ 1.1 TeV,
local (global) significance = 2.6σ (1.0 σ) for *spin-0* and 2.7σ (1.2 σ) for *spin-2*.
Statistically dominated results, systematic effects up to ~16%, mostly from background modeling

Publication: ATL-PHYS-PUB-2021-031/
R. Joshi's poster

Summary

Non-resonant

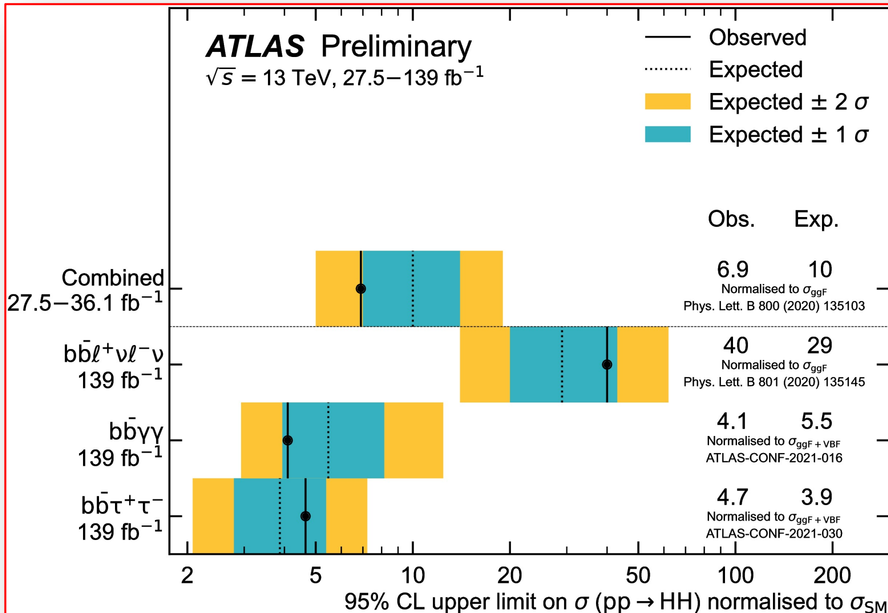

Single channels are now even better than the 36 fb^{-1} HH combination!

Resonant

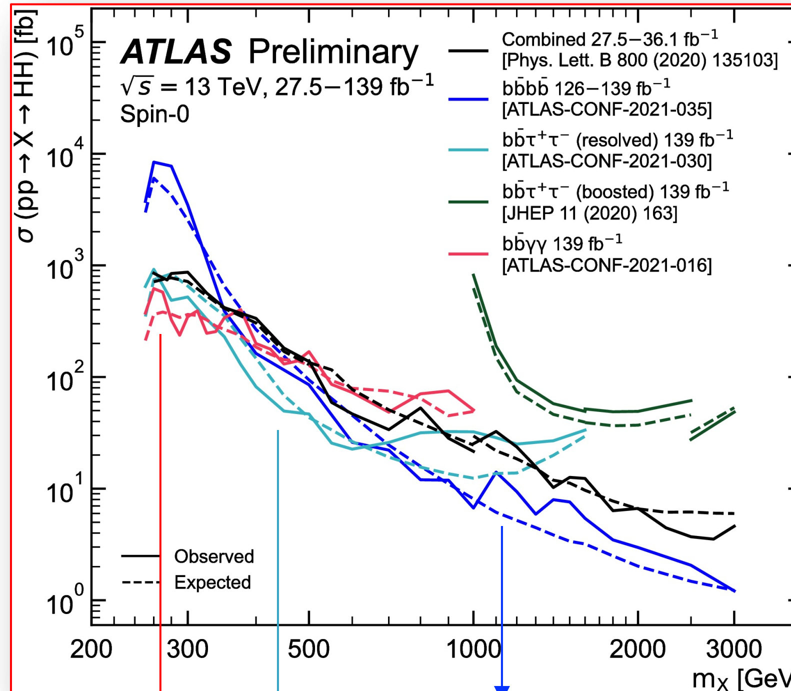

$b\bar{b}\gamma\gamma$ dominates the sensitivity at low m_X

$b\bar{b}b\bar{b}$ dominates the sensitivity at high m_X

$b\bar{b}\tau\tau$ dominates the sensitivity at medium m_X

- Great **analysis improvements** in all final states compared to early Run 2
- **Run 3 could already be a game changer** for a first statistically significant evidence of HH

(old) HL-LHC projections ATL-PHYS-PUB-2020-005

Channel	Statistical-only	Statistical + Systematic
$HH \rightarrow b\bar{b}b\bar{b}$	1.2	0.5
$HH \rightarrow b\bar{b}\tau^+\tau^-$	2.3	2.0
$HH \rightarrow b\bar{b}\gamma\gamma$	2.1	2.0
Combined	3.3 σ	2.9 σ

Thanks for your attention!

Valentina Cairo

SLAC NATIONAL ACCELERATOR LABORATORY

Extra Slides

Physics Motivations

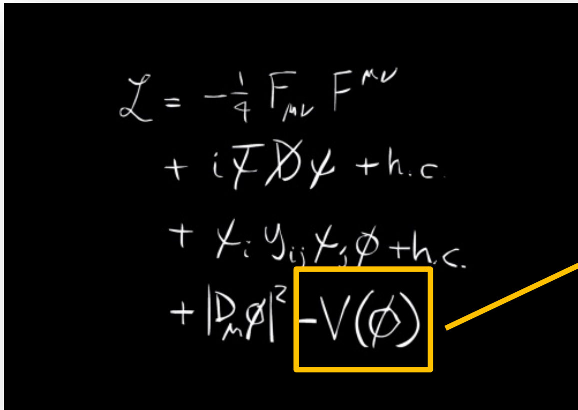

$$V(\phi^\dagger\phi) = \mu^2\phi^\dagger\phi + \lambda(\phi^\dagger\phi)^2$$
$$\supset \lambda v^2 H^2 + \lambda v H^3 + \frac{\lambda}{4} H^4$$

$m_H = \sqrt{2\lambda v^2}$

$v \simeq 246$ GeV.

Known m_H,
we know λ (~0.13)

$\kappa_\lambda = \lambda_{HHH}/\lambda_{SM}$

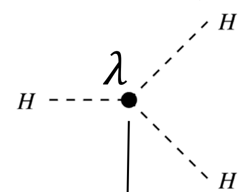

Direct access in HH pairs

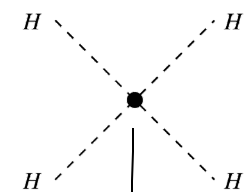

Out of reach even for HL-LHC

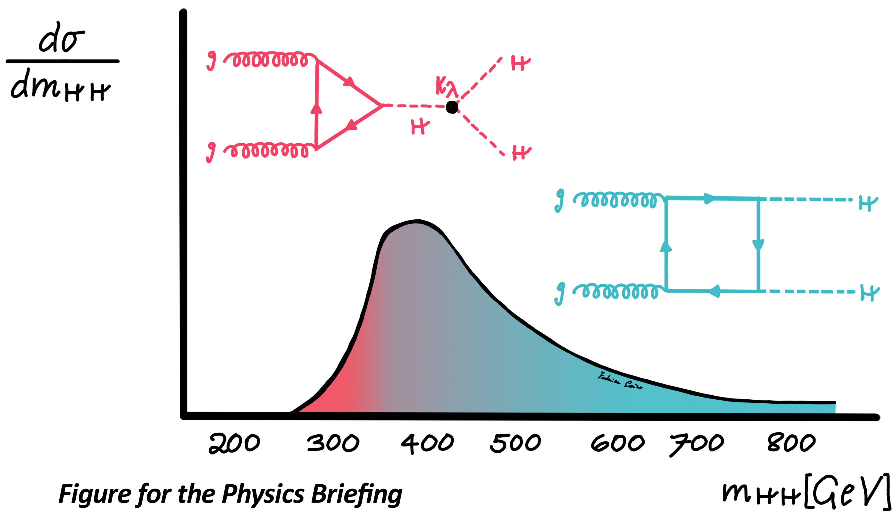

Figure for the Physics Briefing

- Destructive interference between triangle and box diagrams makes the SM σ_{HH} tiny (1000x smaller than single H)
- σ_{HH} and kinematics depend on the coupling modifiers
- New physics can manifest as deviation in σ_{HH}

Non-resonant di-Higgs Production

- **HH** production gives **direct access to the Higgs self-coupling λ**
- Probing the **Higgs-self coupling** is a **key goal of the HL-LHC** programme, but much can be done now!

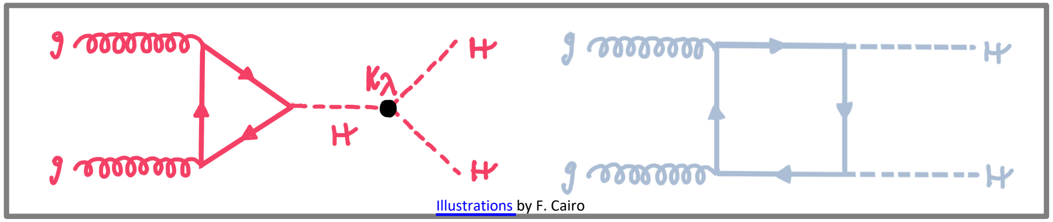

σ_{HH}^{ggF} 31.02 fb at 13 TeV for $m_H = 125.09$ GeV

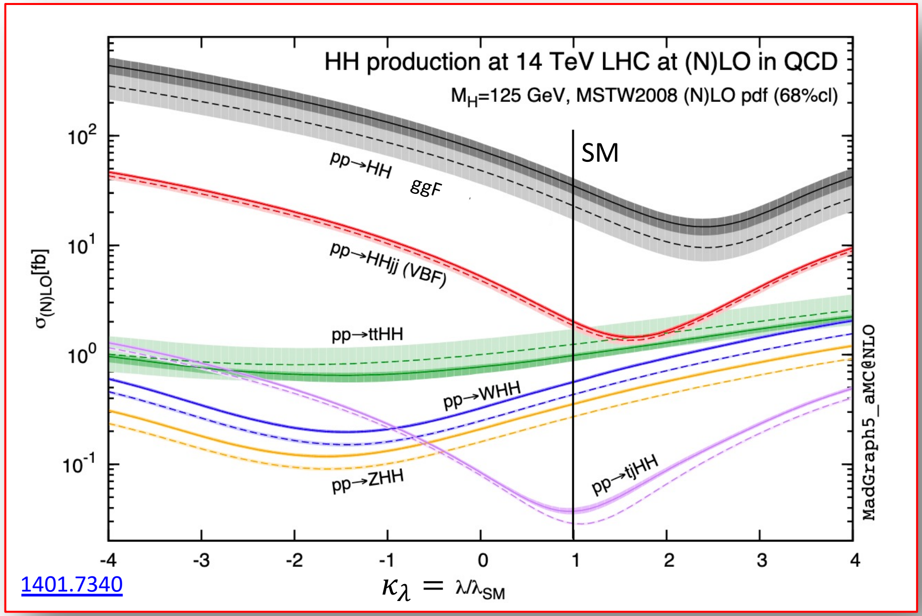

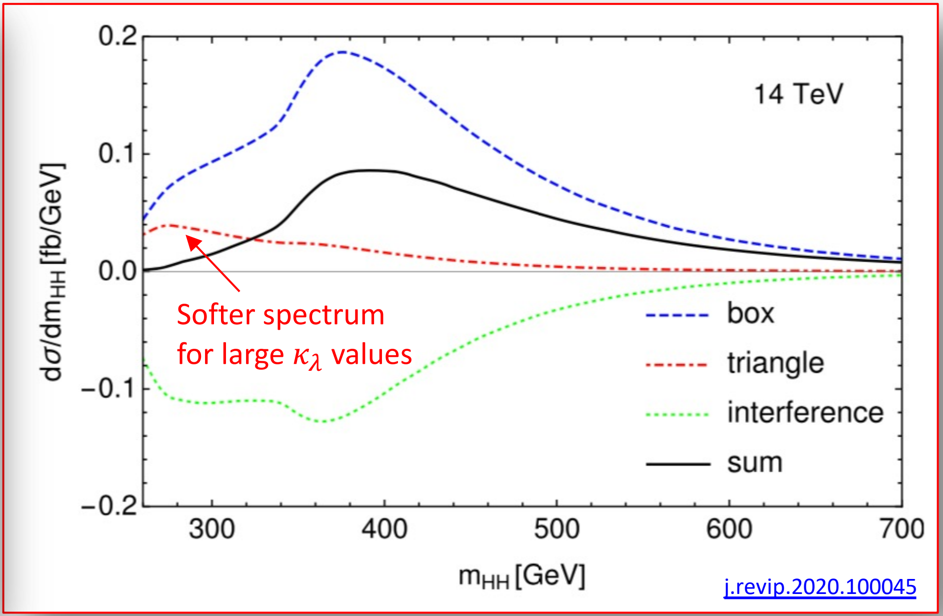

- σ_{HH} and kinematics depend on the coupling modifiers
- New physics can manifest as deviation in σ_{HH}

The Large Hadron Collider

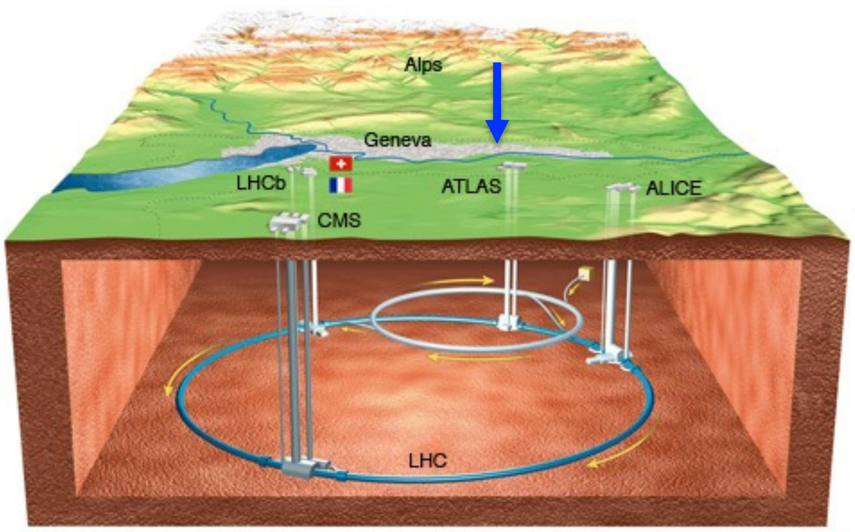

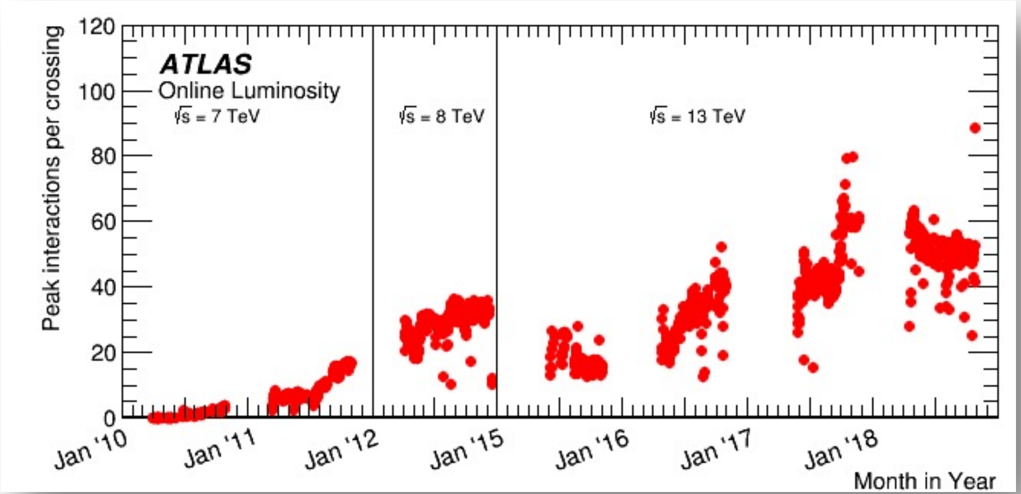

Outperformed specifications during **Run 2**:

- **Peak Luminosity**: x2 (2.14 x 10^{34} $cm^{-2}s^{-1}$)
- **Integrated Luminosity**: 140 fb^{-1}
- **Avg interaction per crossing** $< \mu >$: x2 ($\sim$40)

Two more runs to go:

- **Run 3**: 13/14 TeV, $< \mu > \sim 60$
- **Run 4**: 14 TeV, $< \mu > \sim 200$

The ATLAS Detector

Physics benchmarks drove the design of the detector

- Excellent stand-alone reconstruction capabilities

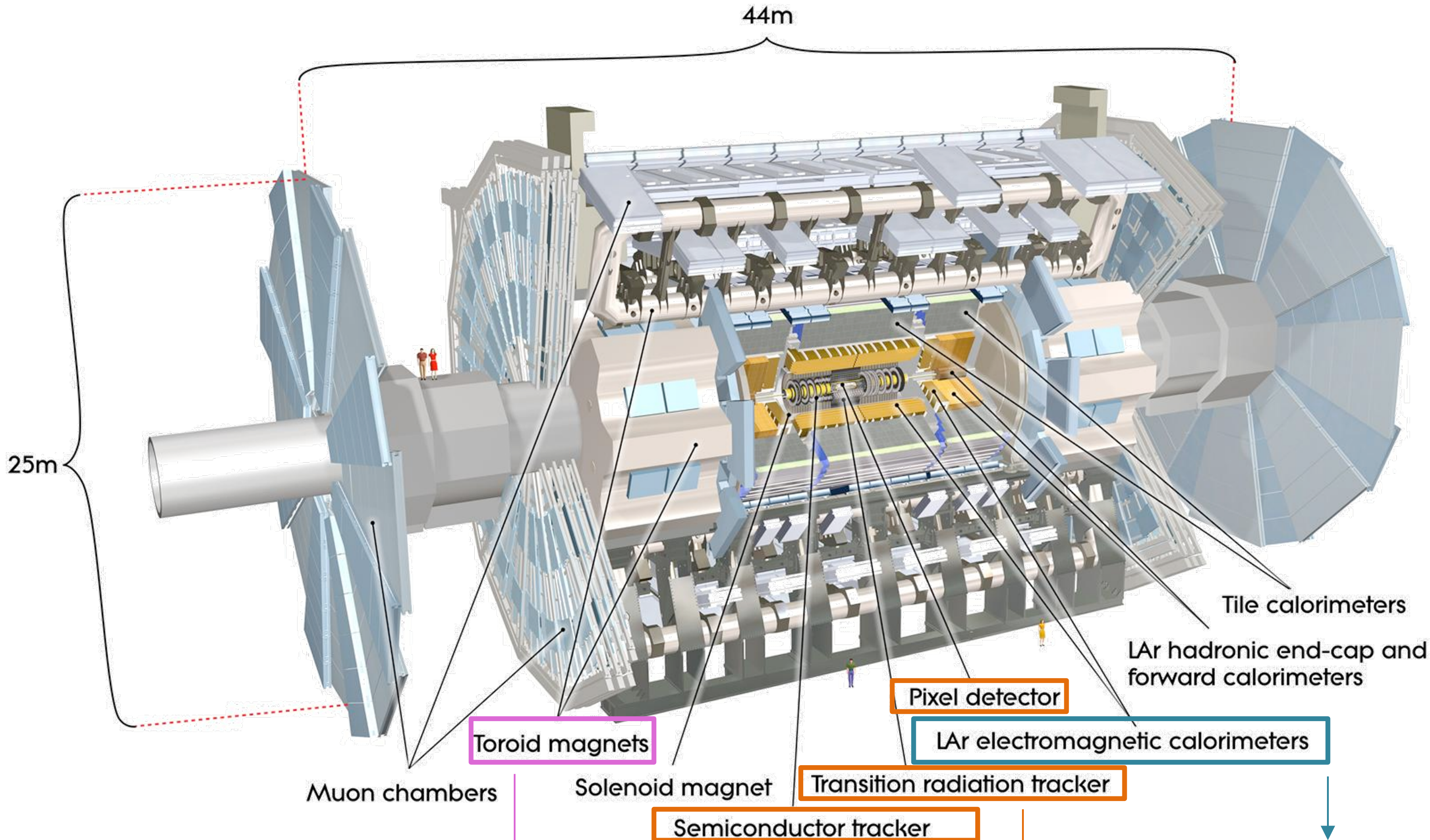

Determines the ATLAS geometry

Combined technologies

maximize $H \rightarrow \gamma\gamma$ sensitivity

What is a b-jet in ATLAS?

High-Level ML b-taggers read **low-level taggers' outputs**

- Impact Parameter based
- Secondary Vertex finding
- **Decay chain Multi-Vertex Algorithm** (JetFitter)

CERN-THESIS-2010-027

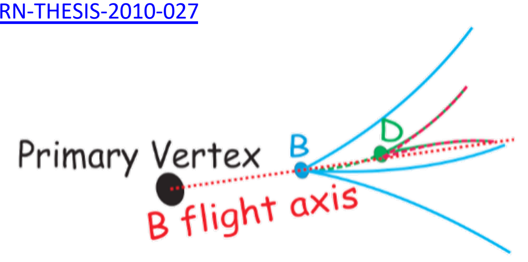

Sensitive to primary vertex reconstruction

Eur. Phys. J. C 79 (2019) 970

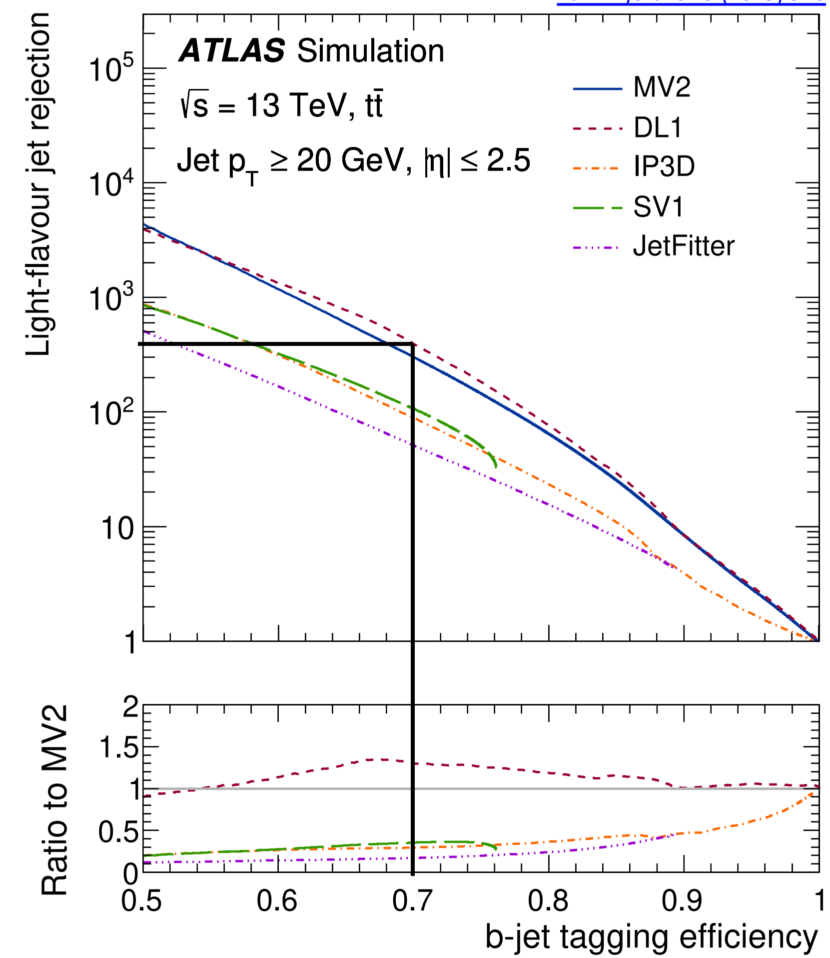

70% b-tag efficiency, ~0.3% light-jet
77% b-tag efficiency, ~1% light-jet

Data and Simulated Samples

- **Full Run 2 data set** (139.0 ± 2.4 fb^{-1})
- **ggF HH signal** ($k_\lambda = 1, 10$) at NLO with **Powheg-Box** v2 PDF4LHC15 + **Pythia 8**
  - Herwig 7 used for PS uncertainty
- **VBF HH signal** ($k_\lambda = 0, 1, 2, 10$) at LO with **MadGraph5_aMC@NLO** v2.6.0 NNPDF3.0nlo + **Pythia 8**
- **Heavy** (251-1000 GeV) **spin 0 resonance** at LO with **MadGraph5_aMC@NLO** v2.6.1 NNPDF2.3lo set of PDFs + **Herwig** v7.1.3
- **Single Higgs** and **continuum backgrounds** summarized in the table below
- Data-driven estimate for ***γ*+jet** and **di-jet** backgrounds
- **PU overlay**: **Pythia 8.1** with NNPDF2.3lo PDF set and **A3** tune

Table 1: Summary of single Higgs boson background samples, split by production modes, and continuum background samples. The generator used in the simulation, the PDF set, and tuned parameters (tune) are also provided.

Process	Generator	PDF set	Showering	Tune
ggF	NNLOPS [61–63] [64, 65]	PDFLHC [38]	Pythia 8.2 [66]	AZNLO [67]
VBF	Powheg-Box v2 [62, 68–75]	PDFLHC	Pythia 8.2	AZNLO
WH	Powheg-Box v2	PDFLHC	Pythia 8.2	AZNLO
$qq \to ZH$	Powheg-Box v2	PDFLHC	Pythia 8.2	AZNLO
$gg \to ZH$	Powheg-Box v2	PDFLHC	Pythia 8.2	AZNLO
$t\bar{t}H$	Powheg-Box v2 [69–71, 75, 76]	NNPDF2.3lo [77]	Pythia 8.2	A14 [78]
bbH	Powheg-Box v2	PDFLHC	Pythia 8.2	A14
$tHqj$	MadGraph5_aMC@NLO	NNPDF3.0nnlo [77]	Pythia 8.2	A14
tHW	MadGraph5_aMC@NLO	NNPDF3.0nnlo [77]	Pythia 8.2	A14
$\gamma\gamma$+jets	Sherpa v2.2.4 [52]	NNPDF3.0nnlo	Sherpa v2.2.4	–
$t\bar{t}\gamma\gamma$	MadGraph5_aMC@NLO	NNPDF2.3lo	Pythia 8.2	–

Object & Event pre-selection

Di-photon triggers with **E_T > 35, 25 GeV**. Trigger efficiency for the non-resonant signal is 82.9% and 69.5% for the resonant signal (using as reference m_X = 300 GeV).

Lepton veto: Events are rejected if they contain medium electrons and/or medium muons

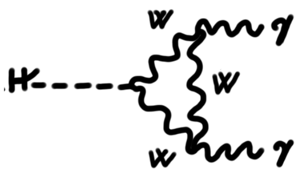

At least **2 photons**:

- Identified (Tight WP)
- Calo- and Track-isolated within a cone of $\Delta R = 0.2$
  - $E_T^{iso} < 0.065 \cdot E_T$ and $p_T^{iso} < 0.05 \cdot E_T$
- 105 GeV < $m\gamma\gamma$ < 160 GeV
- $E_T/m\gamma\gamma$ > 0.35 and 0.25
- **γγ vertex**

$m_{\gamma\gamma}$

Primary Vertex Selection Efficiency

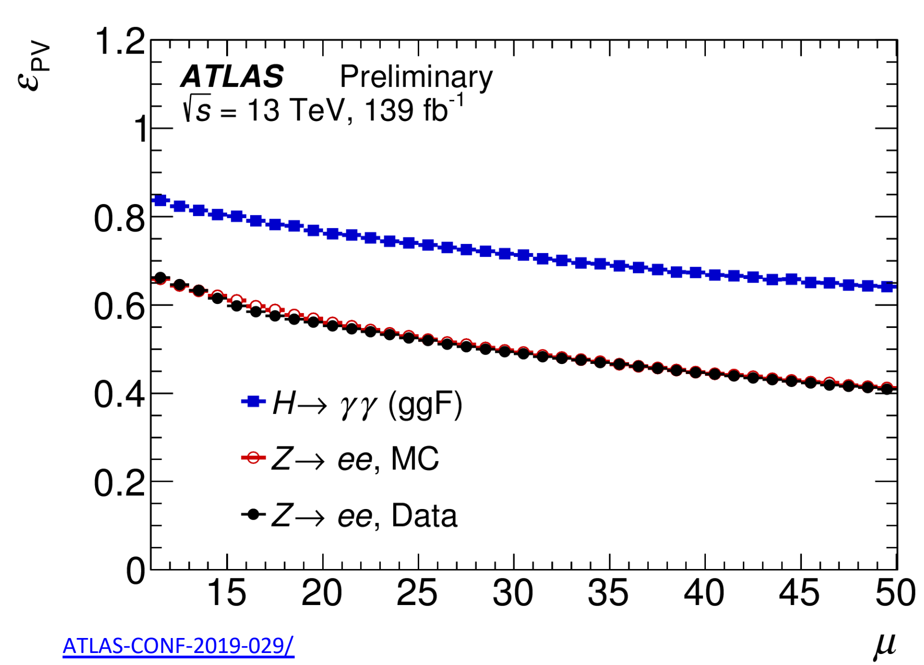

ATLAS-CONF-2019-029/

Object & Event pre-selection

Di-photon triggers with **E_T > 35, 25 GeV**. Trigger efficiency for the non-resonant signal is 82.9% and 69.5% for the resonant signal (using as reference m_X = 300 GeV).

Lepton veto: Events are rejected if they contain medium electrons and/or medium muons

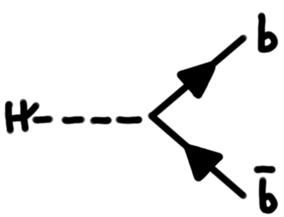

Less than 6 central jets (reduce ttH)

- PFlow jets, anti-kt R=0.4, tight JVT applied

Exactly **2 b-jets**

- DL1r 77% WP
- B-jet energy corrections applied
  - Muon-in-jet
  - pT-reco

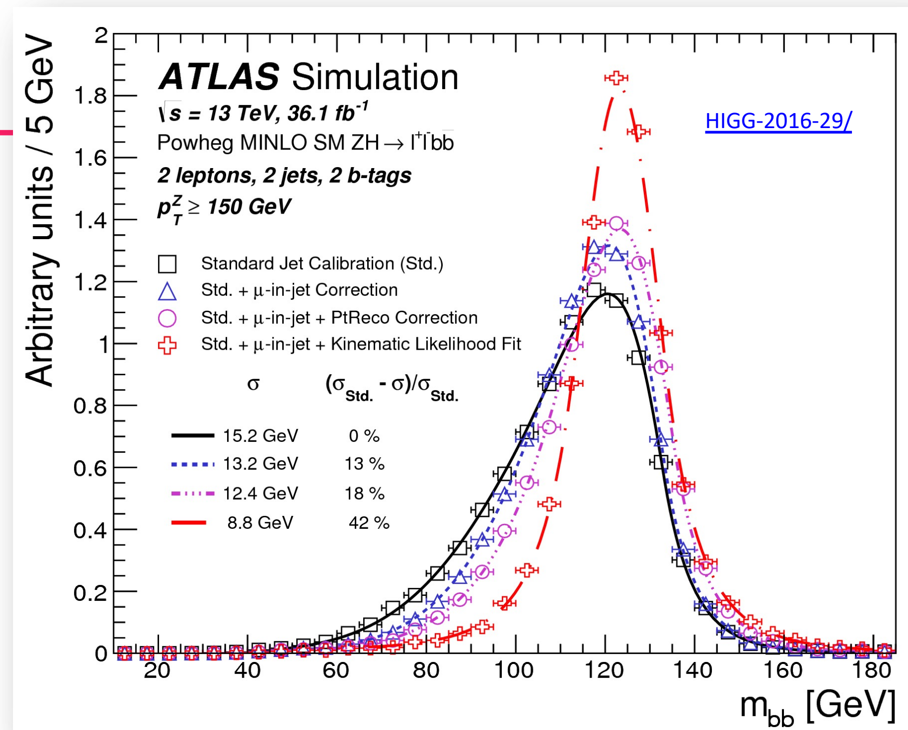

Event Categorization

$$m^*_{b\bar{b}\gamma\gamma} = m_{b\bar{b}\gamma\gamma} - m_{b\bar{b}} - m_{\gamma\gamma} + 250 \text{ GeV}$$

- $m^*_{b\bar{b}\gamma\gamma}$ used in both non-resonant and resonant selections → improves resolution
- **On top of common preselection and $m^*_{b\bar{b}\gamma\gamma}$ cuts, apply BDT-based categorization**
- Require at least 9 expected background events in the **$m\gamma\gamma$ window** (excluding 120-130) to guarantees sufficient events in data side-bands for $m\gamma\gamma$ fit.

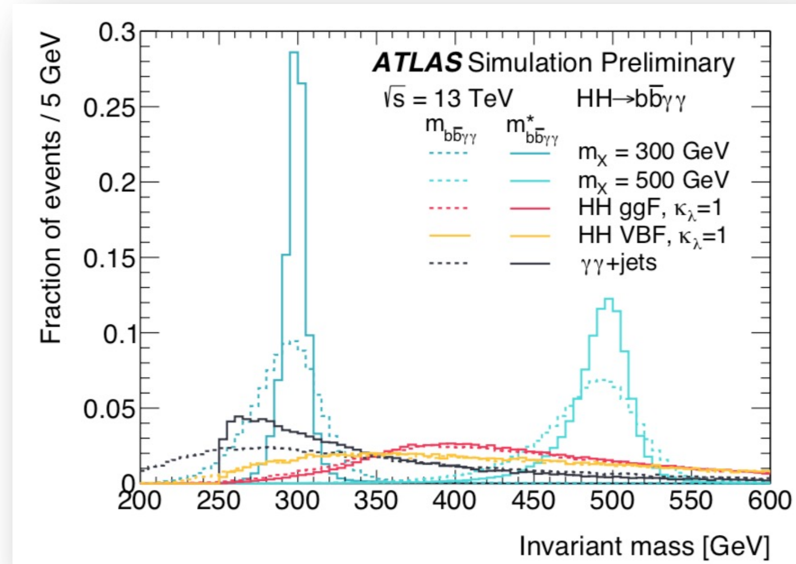

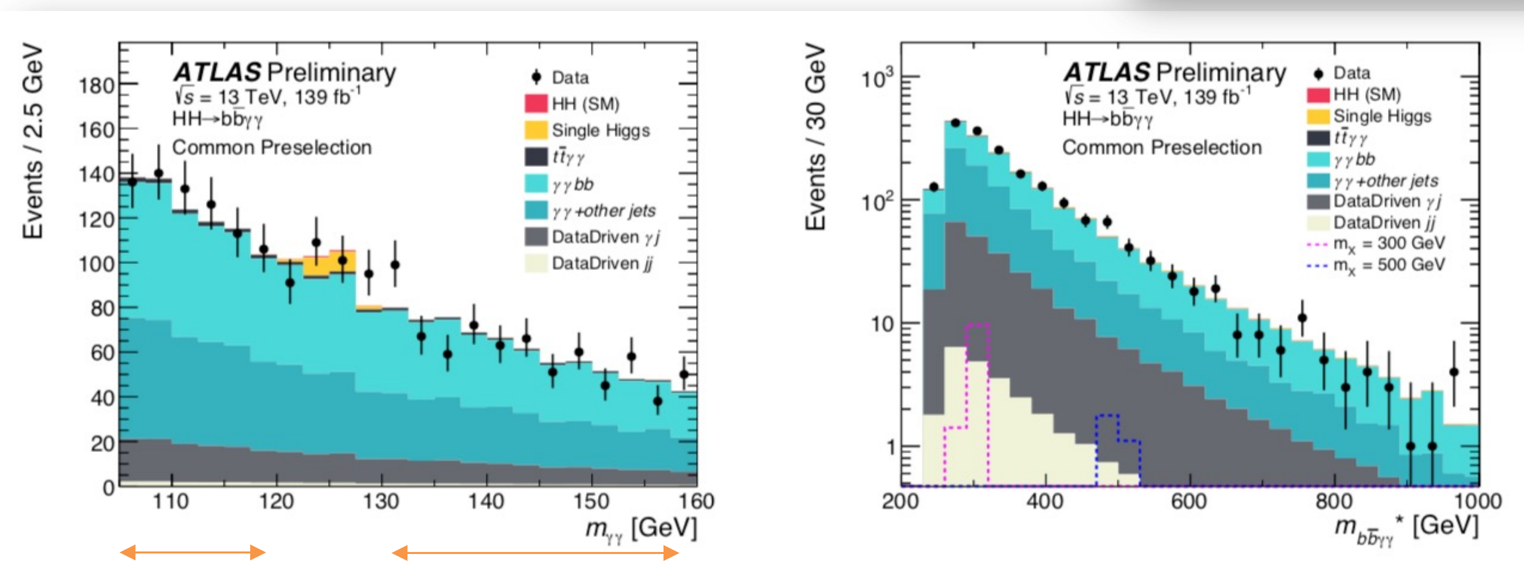

Non-resonant Categorization

4 categories (different wrt previous paper)

- **Low and High $m^*_{b\bar{b}\gamma\gamma}$**
  - **< 350 GeV for BSM**
  - **> 350 GeV for SM**
- In each mass region, train BDT to discriminate signal ($k_\lambda = 1, 10$) from continuum + single Higgs backgrounds
- Photon- and jet-level info used in BDT (details in back-up)
  - m_{bb} very powerful
  - "topness" reduces ttH contamination by ~35%

$$\chi_{Wt} = \min \sqrt{\left(\frac{m_{j_1 j_2} - m_W}{m_W}\right)^2 + \left(\frac{m_{j_1 j_2 j_3} - m_t}{m_t}\right)^2}$$

- **Loose and Tight BDT**
  - Boundaries chosen to maximize combined expected significance

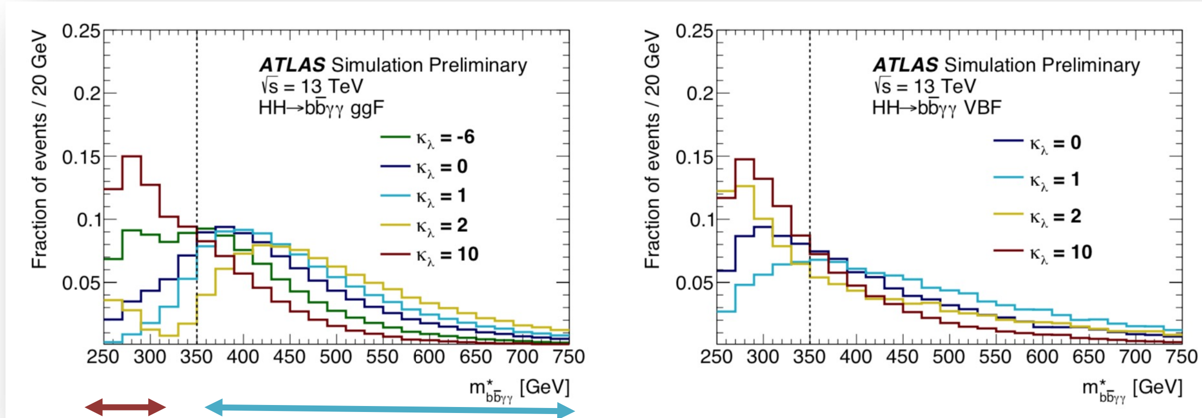

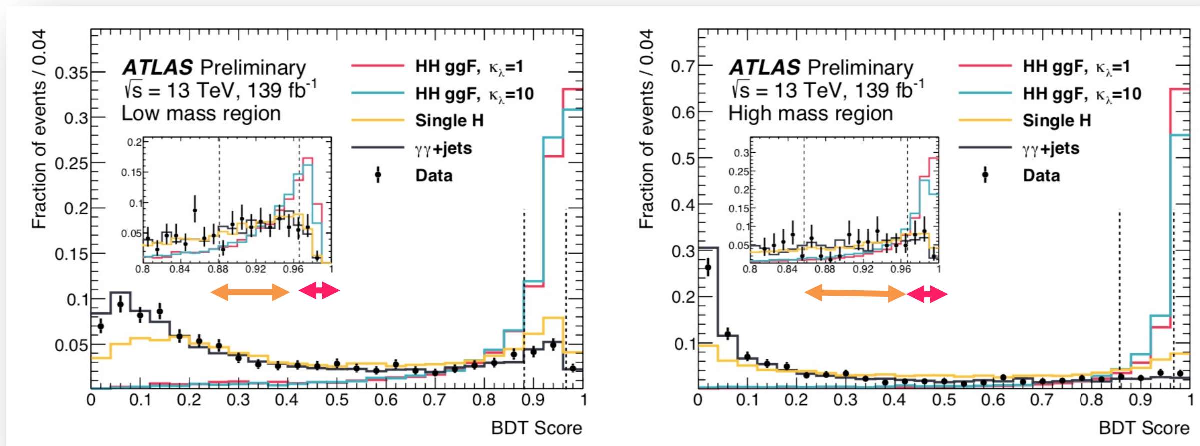

$HH \to b\bar{b}\gamma\gamma$ analysis

Early Run 2 Results
$36.1 fb^{-1}$

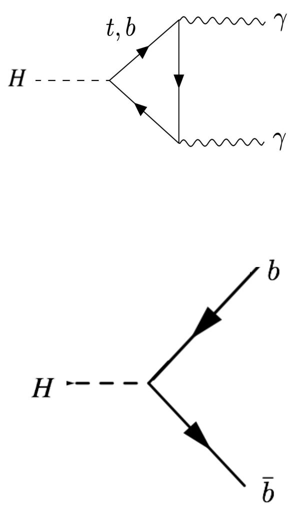

Object selection

Event categorization

Loose (tight) jet selection:

$jet_{pT}^{lead} > 40\ (100)$ GeV

$jet_{pT}^{sub-lead} > 25\ (30)$ GeV

80 (90) GeV < m_{jj} < 140 GeV

1 or 2 b-tag regions:

- 2 b-tag (70%)
- 1 b-tag (60%)

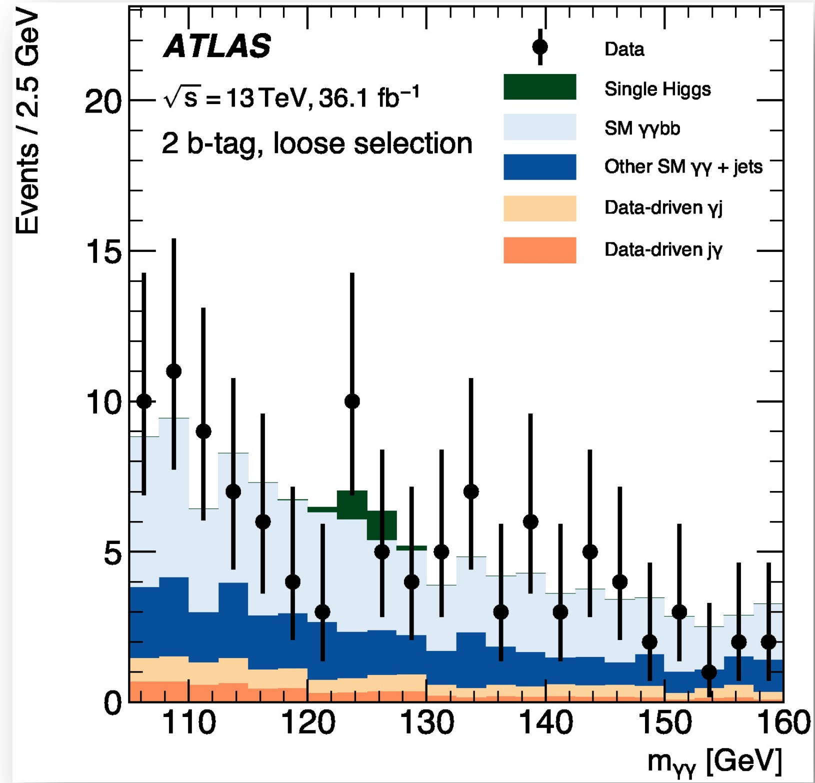

Dominated by γγbb background (no SM measurement exists)

Main SH backgrounds

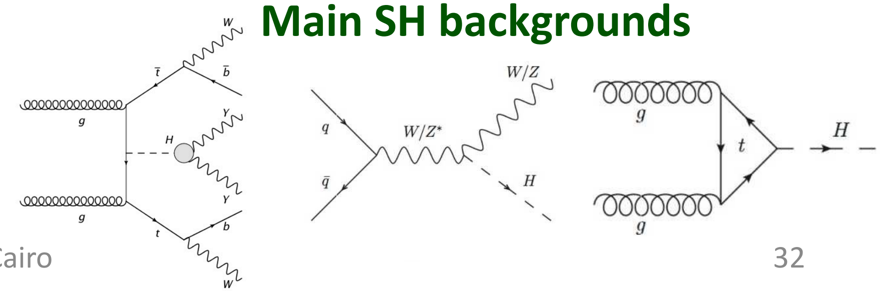

Resonant Categorization

- **Different wrt previous paper**
- **Single BDT for all resonances**
- **2 BDTs** to separate signal from **continuum** and from **single Higgs** backgrounds
- Scores combined in $\mathrm{BDT_{tot}}$

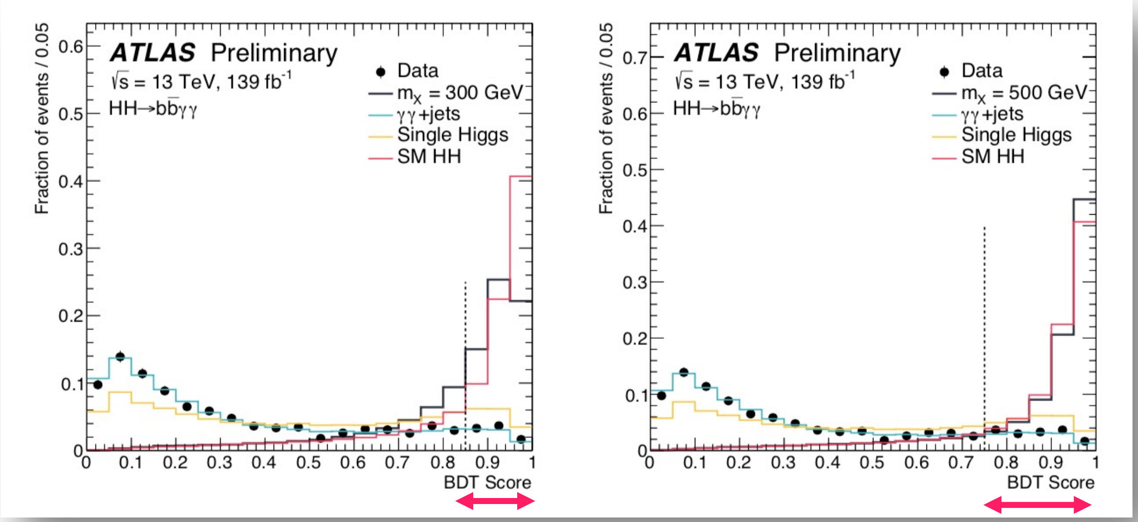

$$\mathrm{BDT_{tot}} = \frac{1}{\sqrt{C_1^2 + C_2^2}} \sqrt{C_1^2 \left(\frac{\mathrm{BDT}_{\gamma\gamma} + 1}{2}\right)^2 + C_2^2 \left(\frac{\mathrm{BDT}_{\mathrm{Single}H} + 1}{2}\right)^2}$$

$$C_1, C_2 \; (C_2 = 1 - C_1)$$

- **2-stage optimization**
  1. Maximize significance for each resonance
     - Different coefficients and BDT scores
  2. Select coefficients providing a significance within 5% from the maximum value, for each resonance
     - A common $C_1 = 0.65$ coefficient is found, individual BDT cuts are used

A cut on $m^*_{b\bar{b}\gamma\gamma}$ is applied at $\pm 2\sigma$ ($\pm 4\sigma$) of the expected mean value for signal events for each resonance (at 900-1000 GeV)

Data/MC comparison

Non-resonant

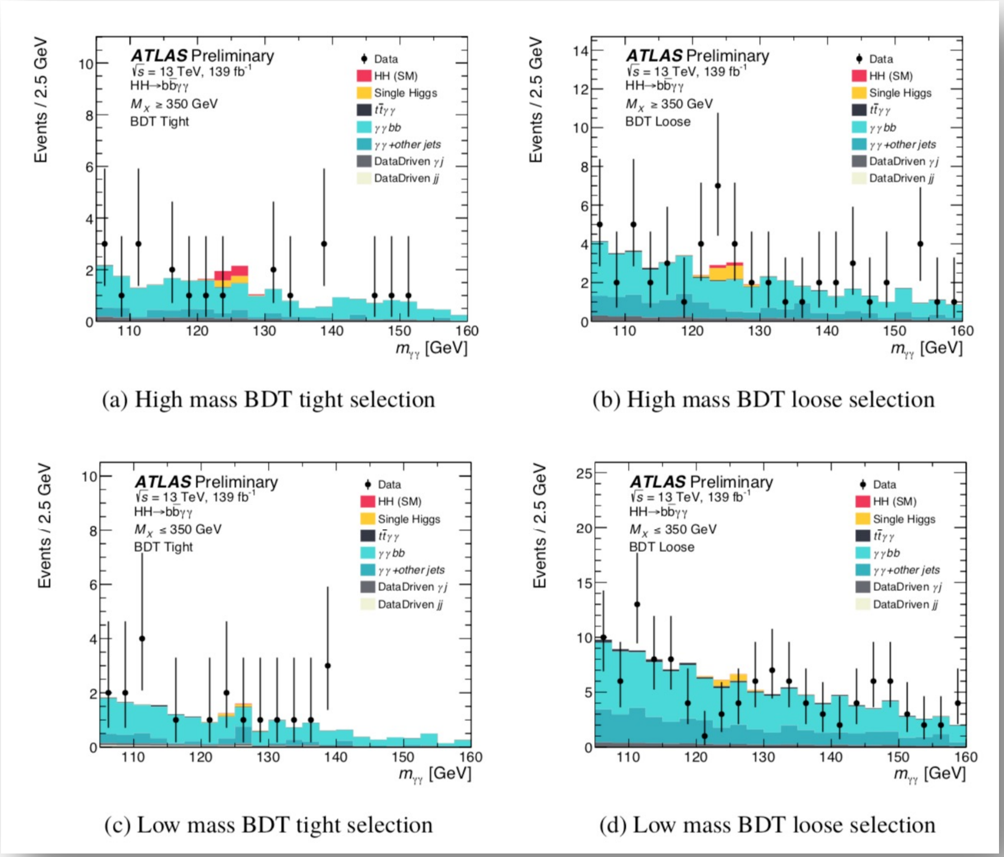

(a) High mass BDT tight selection (b) High mass BDT loose selection

(c) Low mass BDT tight selection (d) Low mass BDT loose selection

Dominated by
γγbb
background
(flavor
composition
from Sherpa)

Data-driven $\gamma\&j$ via 2x2D method based on reverting γ isolation and identification criteria

(only for data/MC comparison)

Resonant

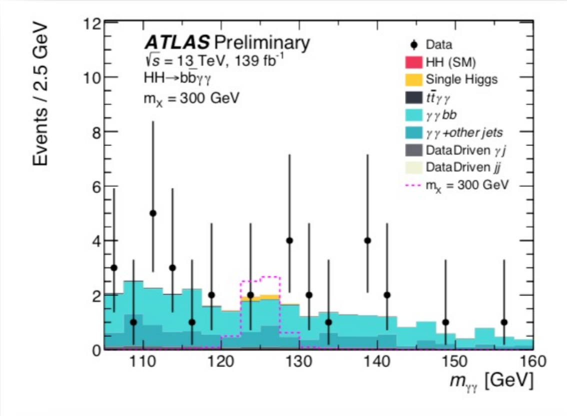

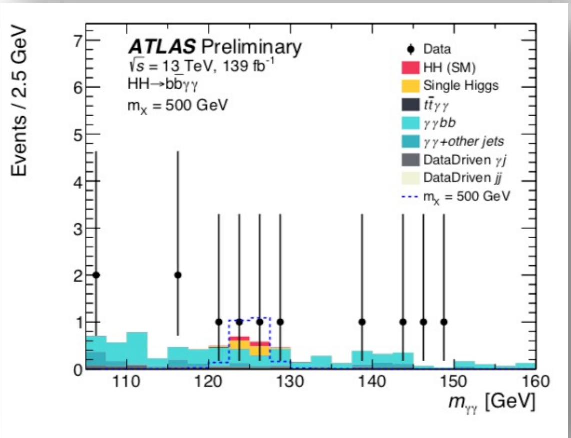

Main SH backgrounds

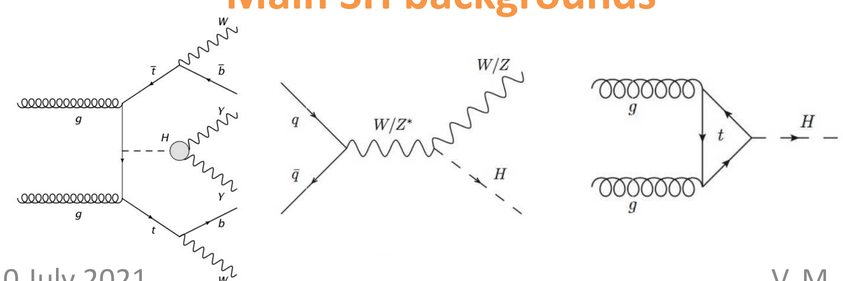

Modeling of the discriminant variable

- $m_{\gamma\gamma}$ for both non-resonant & resonant (different than previous paper, improved resonant limits at low mass thanks to easier background modeling)
- Yields are parameterized with a 2nd order polynomial
- **HH signal and single Higgs background** shape modelled from MC with a **DSCB** function
  - No sizable dependence on k_λ is observed

- **Continuum background** modelled from data side bands
- Systematic uncertainty assigned to the function choice via ***Spurious Signal*** method
  - Estimate signal bias by fitting a background only template with a signal + background function
  - **Exponential function** chosen: similar bias, but minimal number of degrees of freedom
    - Wald test performed in data, no sign of preference for higher degree function

Statistical Analysis

- Maximum likelihood fit of $m_{\gamma\gamma}$ in 105 GeV < $m_{\gamma\gamma}$ < 160 GeV, performed simultaneously over all categories

$$\mathcal{L} = \prod_{c} \left(\mathrm{Pois}(n_c | N_c(\boldsymbol{\theta})) \cdot \prod_{i=1}^{n_c} f_c(m^i_{\gamma\gamma}, \boldsymbol{\theta}) \cdot G(\boldsymbol{\theta}) \right)$$

Expected #events

$$N_c(\boldsymbol{\theta}) = \mu \cdot N_{HH,c}(\boldsymbol{\theta}^{\text{yield}}_{HH}) + N^{\text{res}}_{\text{bkg,c}}(\boldsymbol{\theta}^{\text{yield}}_{\text{res}}) + N_{\text{SS,c}} \cdot \boldsymbol{\theta}^{\text{SS,c}} + N^{\text{non-res}}_{\text{bkg,c}}$$

PDF

$$f_c(m_{\gamma\gamma}, \boldsymbol{\theta}) = [\mu \cdot N_{HH,c}(\boldsymbol{\theta}^{\text{yield}}_{HH}) \cdot f_{HH,c}(m_{\gamma\gamma}, \boldsymbol{\theta}^{\text{shape}}_{HH}) + N^{\text{res}}_{\text{bkg,c}}(\boldsymbol{\theta}^{\text{yield}}_{\text{res}}) \cdot f^{\text{res}}_{\text{bkg,c}}(m_{\gamma\gamma}, \boldsymbol{\theta}^{\text{shape}}_{\text{res}}) + N_{\text{SS,c}} \cdot \boldsymbol{\theta}^{\text{SS,c}}_{HH} \cdot f_{HH,c}(m_{\gamma\gamma}, \boldsymbol{\theta}^{\text{shape}}_{HH}) + N^{\text{non-res}}_{\text{bkg,c}} \cdot f^{\text{non-res}}_{\text{bkg,c}}(m_{\gamma\gamma}, \boldsymbol{\theta}^{\text{shape}}_{\text{non-res}})] / N_c(\boldsymbol{\theta}^{\text{yield}}_{\text{non-res}})$$

Single Higgs yields fixed to SM values, while μ, non-resonant background shape and nuisance parameters for sys. floating in fit

Non-resonant

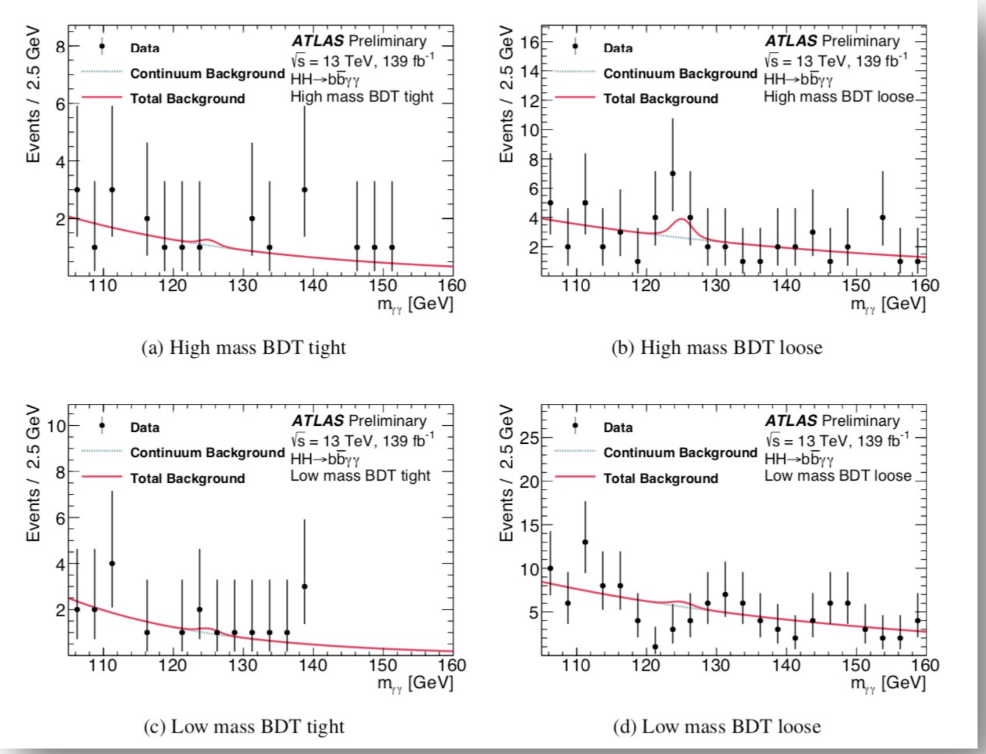

(a) High mass BDT tight
(b) High mass BDT loose
(c) Low mass BDT tight
(d) Low mass BDT loose

Resonant

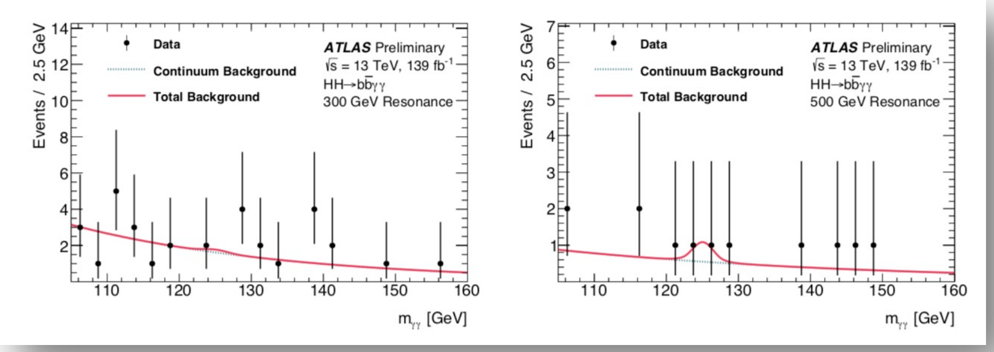

Non-resonant results

No signal is observed, exclusion limits are set via the CLs method with asymptotic approximation

- Observed non-resonant HH production of **130 fb**, while **180 fb** is expected.
  - **4.1 (5.5) x the SM**

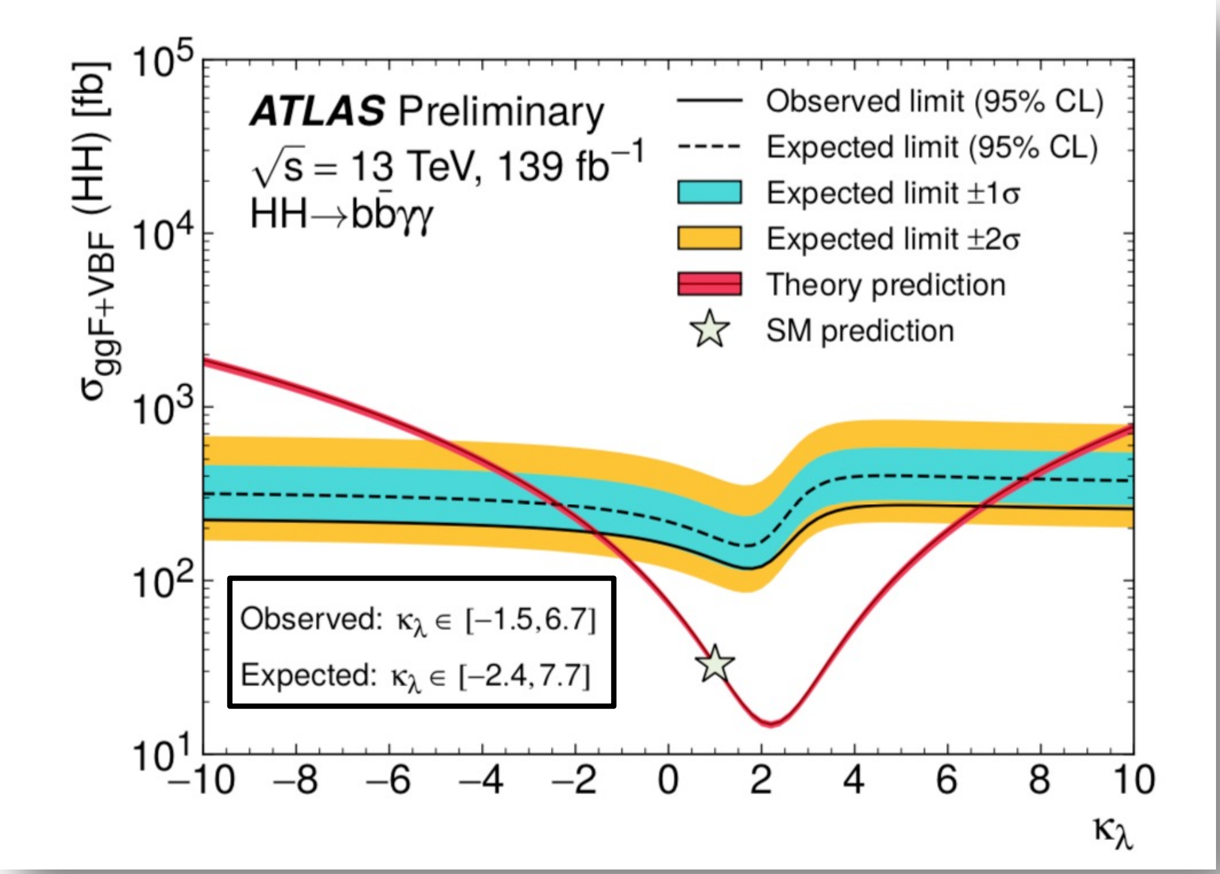

- 36 fb^{-1} results: **22 (28) x SM** observed (expected), $-8.2\ (-8.3) < k_\lambda < 13.2\ (13.2)$
- **Full Run 2 CMS results: 7.7 (5.2) x SM,** $-3.3\ (-2.5) \leq k_\lambda \leq 8.5\ (8.2)$

Resonant $HH \rightarrow b\bar{b}\gamma\gamma$

- **Different analysis strategy** compared to the early Run 2 analysis
- **single BDT for all resonances, 2 BDTs** to separate signal from **continuum** and from **single Higgs** backgrounds, scores combined in $\mathrm{BDT_{tot}}$

$$\mathrm{BDT_{tot}} = \frac{1}{\sqrt{C_1^2 + C_2^2}} \sqrt{C_1^2 \left(\frac{\mathrm{BDT}_{\gamma\gamma} + 1}{2}\right)^2 + C_2^2 \left(\frac{\mathrm{BDT}_{\mathrm{Single}H} + 1}{2}\right)^2}$$

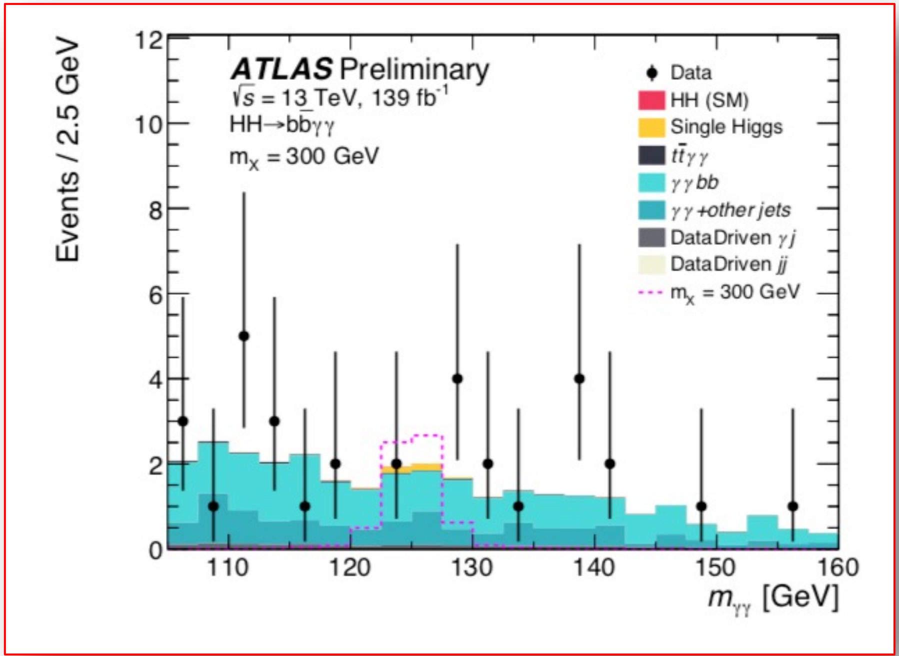

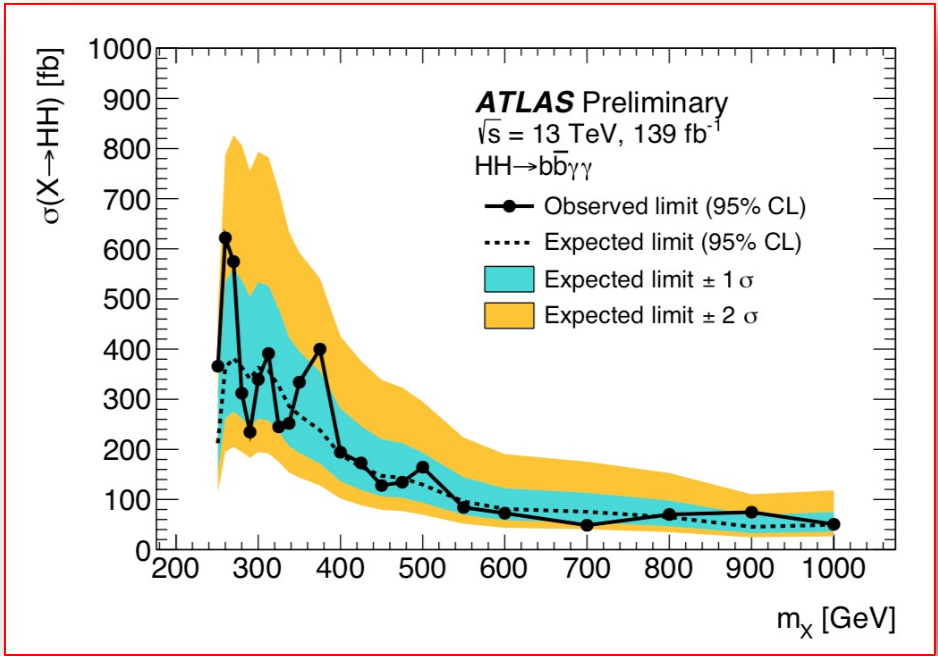

- **~ 30% improvement from BDT strategy, lower mass regime tested**
- 36 fb^{-1} results: Observed (expected) limits between **1.1 pb (0.9 pb) and 0.12 pb (0.15 pb)** in the range **260 GeV < m_X < 1000 GeV**.

Resonant results

No signal is observed, exclusion limits are set via the CLs method with asymptotic approximation

- Observed and expected σ upper limits at 95% CL on the for a narrow width scalar resonance varying between **610–47 fb (360–43 fb)** in **251 GeV ≤ m_X ≤ 1000 GeV**.

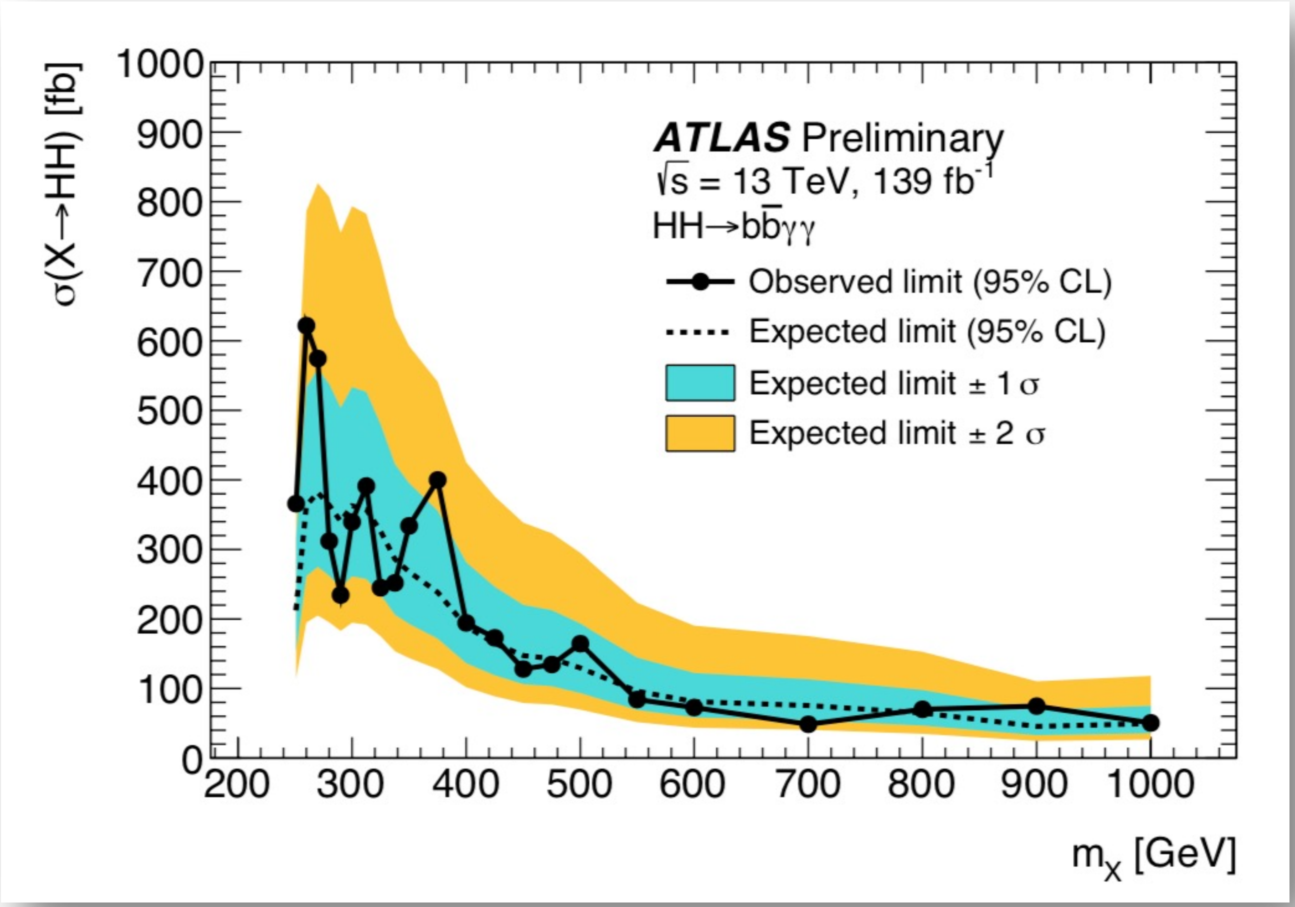

- 36 fb^{-1} results: Observed (expected) limits between **1.1 pb (0.9 pb) and 0.12 pb (0.15 pb)** in the range **260 GeV < m_X < 1000 GeV**.

Systematic Uncertainties

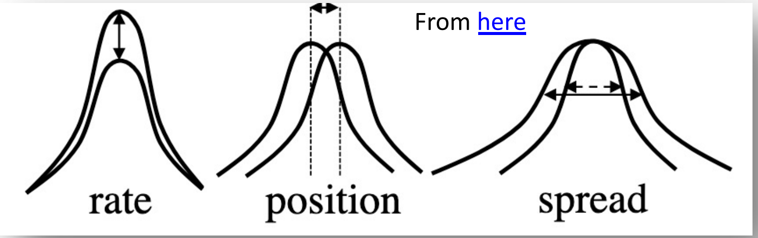

- **Statistically dominated analysis, systematics have a sub-dominant effect**
- Luminosity uncertainty 1.7%
- Continuum background fitted from data, only spurious signal uncertainty
- Experimental & theory systematics affect HH non-resonant, HH resonant and Single Higgs

		Relative impact of the systematic uncertainties in %	
Source	Type	Non-resonant analysis HH	Resonant analysis $m_X = 300$ GeV
Experimental			
Photon energy scale	Norm.+Shape	5.2	2.7
Photon energy resolution	Norm.+Shape	1.8	1.6
Flavor tagging	Normalization	0.5	< 0.5
Theoretical			
Heavy flavor content	Normalization	1.5	< 0.5
Higgs boson mass	Norm.+Shape	1.8	< 0.5
PDF+α_S	Normalization	0.7	< 0.5
$\boxed{\text{Spurious signal}}$	Normalization	5.5	5.4

$HH \rightarrow b\bar{b}\tau\tau$ analysis (1)

Relatively large BR and **clean final state** (cleaner compared to e.g. 4b)

SingleTau (80<pT<160 GeV)/**DiTau** (35-25 GeV) **triggers for $\tau_{had}\,\tau_{had}$**

SingleLepton (e: 24<E_T<26 GeV, μ: 20<p_T<26 GeV) **/Lepton** (e: E_T>17 GeV, μ: p_T>14 GeV)**+Tau** (μ: p_T>25 GeV) **triggers in $\tau_{lep}\,\tau_{had}$**

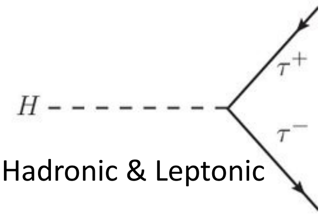

Hadronic & Leptonic

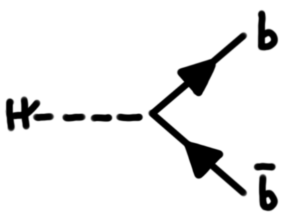

77% btag WP (~1% mistag)
Muon-in-jet+pTReco

Object selection

See extra slides for details on object selection

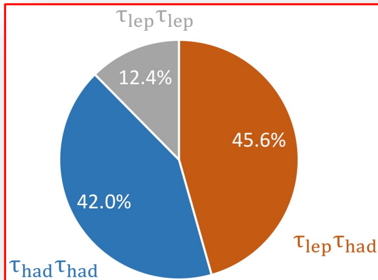

Event categorization

MVA in 3 categories:

$\tau_{had}\,\tau_{had}$ (opp. charged) → High Purity

$\tau_{lep}\,\tau_{had}$ (e/μ & opp. charged τ)

LTT → Low mass sensitivity due to low p_T^l

SLT → High acceptance, large ttbar background

Control region for Z+HF (mll)

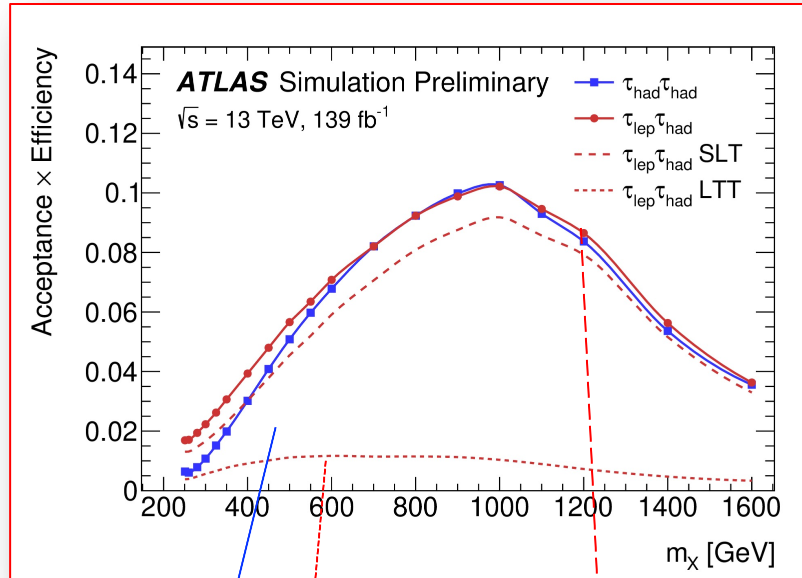

$HH \to b\bar{b}\tau\tau$ analysis (3)

Z+HF & ttbar normalization from mll fit to data

Fake taus:
Fake factor method for $\tau_{lep}\ \tau_{had}$ and $\tau_{had}\ \tau_{had}$ (multi-jet), scale factors for $\tau_{had}\ \tau_{had}$ ttbar

Background modeling

$\tau_{lep}\ \tau_{had}$

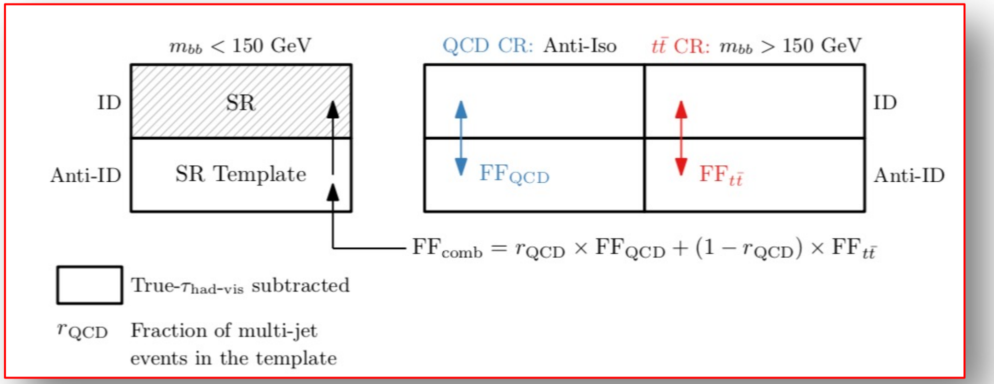

$\tau_{had}\ \tau_{had}$, multi-jet

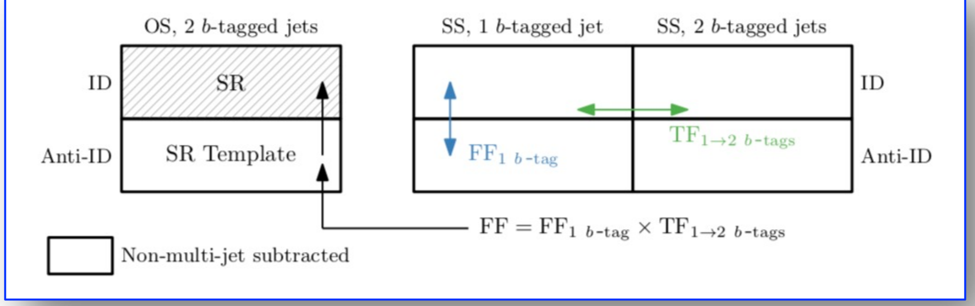

$\tau_{had}\ \tau_{had}$, ttbar

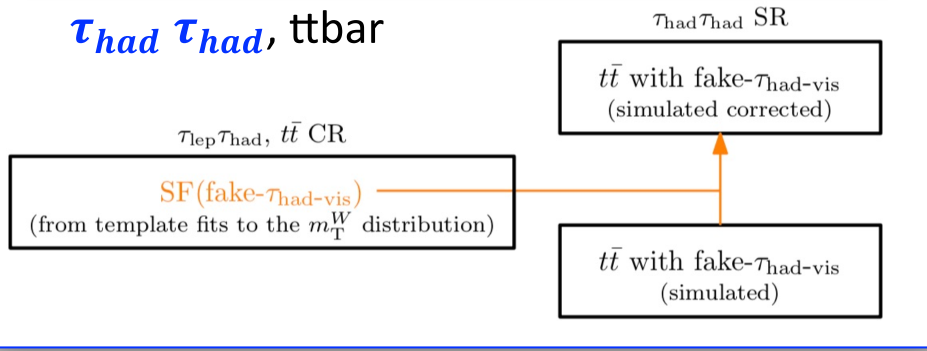

$HH \to b\bar{b}\tau\tau$

Table 1: The generators used for the simulation of the signal and background processes. If not specified, the order of the cross-section calculation refers to the expansion in the strong coupling constant (α_S). The acronyms ME, PS and UE are used for matrix element, parton shower and underlying event, respectively.

The resonant *HH* signal was simulated for 19 values of the resonance mass, m_X, between 251 GeV and 1.6 TeV.

Process	ME generator	ME PDF	PS and hadronisation	UE model tune	Cross section order
Signal					
non-resonant $gg \to HH$ (ggF)	Powheg-Box v2	PDF4LHC15 [73]	Pythia 8.244 [68]	A14	NNLO FTApprox [20]
non-resonant $qq \to qqHH$ (VBF)	MadGraph	NNPDF3.0NLO [74]	Pythia 8.244	A14	N3LO(QCD)
resonant $gg \to X \to HH$	MadGraph	NNPDF2.3LO [70]	Herwig v7.1.3	H7.1-Default	–
Top-quark					
$t\bar{t}$	Powheg-Box v2	NNPDF3.0NLO	Pythia 8.230	A14	NNLO+NNLL [75]
t-channel	Powheg-Box v2	NNPDF3.0NLO	Pythia 8.230	A14	NLO [76]
s-channel	Powheg-Box v2	NNPDF3.0NLO	Pythia 8.230	A14	NLO [77]
Wt	Powheg-Box v2	NNPDF3.0NLO	Pythia 8.230	A14	NLO [78]
$t\bar{t}V$ ($V = W, Z$)	Sherpa 2.2.1	NNPDF3.0NNLO [74]	Sherpa 2.2.1	Default	NLO
Vector boson + jets					
W+jets	Sherpa 2.2.1	NNPDF3.0NNLO	Sherpa 2.2.1	Default	NNLO
Z+jets	Sherpa 2.2.1	NNPDF3.0NNLO	Sherpa 2.2.1	Default	NNLO
Diboson					
WW	Sherpa 2.2.1	NNPDF3.0NNLO	Sherpa 2.2.1	Default	NLO
WZ	Sherpa 2.2.1	NNPDF3.0NNLO	Sherpa 2.2.1	Default	NLO
ZZ	Sherpa 2.2.1	NNPDF3.0NNLO	Sherpa 2.2.1	Default	NLO
Single Higgs boson					
ggF	Powheg-Box v2	NNPDF3.0NLO	Pythia 8.212	AZNLO	N3LO(QCD)+NLO(EW) [79–83]
VBF	Powheg-Box v2	NNPDF3.0NLO	Pythia 8.212	AZNLO	NNLO(QCD)+NLO(EW)
$qq \to WH$	Powheg-Box v2	NNPDF3.0NLO	Pythia 8.212	AZNLO	NNLO(QCD)+NLO(EW) [84–90]
$qq \to ZH$	Powheg-Box v2	NNPDF3.0NLO	Pythia 8.212	AZNLO	NNLO(QCD)+NLO(EW)
$gg \to ZH$	Powheg-Box v2	NNPDF3.0NLO	Pythia 8.212	AZNLO	NLO+NLL
ttH	Powheg-Box v2	NNPDF3.0NLO	Pythia 8.230	A14	NLO

$HH \rightarrow b\bar{b}\tau\tau$ selection

Table 2: Summary of the event selection, shown separately in the different trigger categories. In cases where pairs of reconstructed objects of the same type are required, thresholds on the (sub-)leading p_T object are given outside (within) parentheses. When the selection depends on the year of data-taking, the possible values of the requirements are separated by commas, except for the jet selection in the lepton-plus-$\tau_{\text{had-vis}}$ trigger and di-$\tau_{\text{had-vis}}$ triggers which use multiple possible selection criteria, that are described in Section 5.1. The p_T trigger thresholds shown correspond to the offline requirements.

$\tau_{had}\tau_{had}$ channel		$\tau_{lep}\tau_{had}$ channel	
STT	DTT	SLT	LTT
e/μ selection			
No loose e/μ with $p_T > 7$ GeV		Exactly one tight e or medium μ	
		$p_T^e > 25, 27$ GeV	18 GeV $< p_T^e <$ SLT cut
		$p_T^\mu > 21, 27$ GeV	15 GeV $< p_T^\mu <$ SLT cut
		$\lvert\eta^e\rvert < 2.47$, not $1.37 < \lvert\eta^e\rvert < 1.52$	
		$\lvert\eta^\mu\rvert < 2.7$	
$\tau_{\text{had-vis}}$ selection			
Two loose $\tau_{\text{had-vis}}$		One loose $\tau_{\text{had-vis}}$	
$\lvert\eta\rvert < 2.5$		$\lvert\eta\rvert < 2.3$	
$p_T > 100, 140, 180$ (25) GeV	$p_T > 40$ (30) GeV	$p_T > 20$ GeV	$p_T > 30$ GeV
Jet selection			
≥ 2 jets with $\lvert\eta\rvert < 2.5$			
$p_T > 45$ (20) GeV	Trigger dependent	$p_T > 45$ (20) GeV	Trigger dependent
Event-level selection			
Trigger requirements passed			
Collision vertex reconstructed			
$m_{\tau\tau}^{\text{MMC}} > 60$ GeV			
Opposite-sign electric charges of $e/\mu/\tau_{\text{had-vis}}$ and $\tau_{\text{had-vis}}$			
Exactly two b-tagged jets			
		$m_{bb} < 150$ GeV	

- LepHad: largely dominated by $t\bar{t}$
  - Preselection signal efficiency: ~ 5%
- HadHad: significant contributions from $t\bar{t}$ (+ fakes) , Z + jets, QCD fakes
  - Pre-selection signal efficiency: ~ 4%

$HH \to b\bar{b}\tau\tau$ MVA

Table 3: Variables used as inputs to the MVAs in the three analysis categories. The same choice of input variables is used for the resonant and non-resonant production modes. The variables are defined in the main text.

Variable	$\tau_{\rm had}\tau_{\rm had}$	$\tau_{\rm lep}\tau_{\rm had}$ SLT	$\tau_{\rm lep}\tau_{\rm had}$ LTT
m_{HH}	✓	✓	✓
$m_{\tau\tau}^{\rm MMC}$	✓	✓	✓
m_{bb}	✓	✓	✓
$\Delta R(\tau,\tau)$	✓	✓	✓
$\Delta R(b,b)$	✓	✓	
$\Delta p_{\rm T}(\ell,\tau)$		✓	✓
Sub-leading b-tagged jet $p_{\rm T}$		✓	
$m_{\rm T}^{W}$		✓	
$E_{\rm T}^{\rm miss}$		✓	
$E_{\rm T}^{\rm miss}$ ϕ centrality		✓	
$\Delta\phi(\tau\tau, bb)$		✓	
$\Delta\phi(\ell, E_{\rm T}^{\rm miss})$			✓
$\Delta\phi(\ell\tau, E_{\rm T}^{\rm miss})$			✓
$S_{\rm T}$			✓

$HH \rightarrow b\bar{b}\tau\tau$ background

$\tau_{lep}\,\tau_{had}$

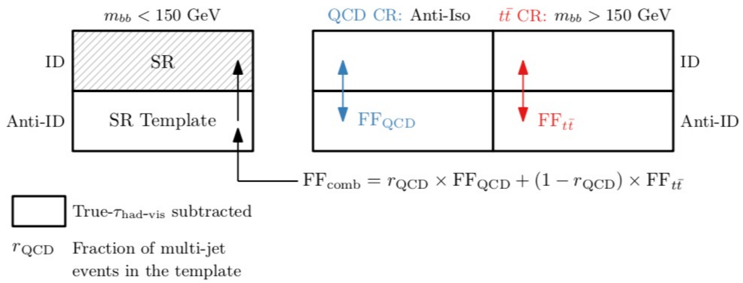

Figure 4: Schematic depiction of the combined fake-factor method used to estimate multi-jet and $t\bar{t}$ background with fake-$\tau_{\text{had-vis}}$ in the $\tau_{\text{lep}}\tau_{\text{had}}$ channel. Backgrounds which are not from events with fake-$\tau_{\text{had-vis}}$ originating from jets are subtracted from data in all control regions. Events in which an electron or a muon is misidentified as a $\tau_{\text{had-vis}}$ are also subtracted, but their contribution is very small. Both sources are indicated by "True-$\tau_{\text{had-vis}}$ subtracted" in the legend.

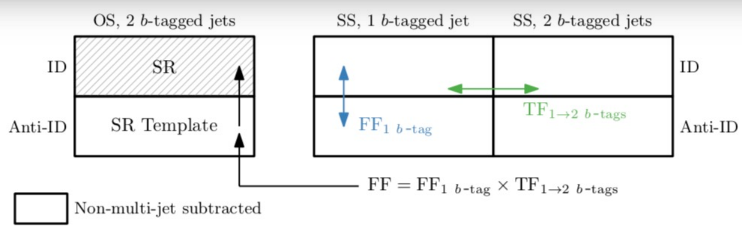

$\tau_{had}\,\tau_{had}$

Figure 5: Schematic depiction of the combined fake-factor method to estimate multi-jet background with fake-$\tau_{\text{had-vis}}$ in the $\tau_{\text{had}}\tau_{\text{had}}$ channel. Backgrounds with true-$\tau_{\text{had-vis}}$ which are not from multi-jet events are simulated and subtracted from data in all the control regions. This is indicated by "Non-multi-jet subtracted" in the legend.

$\tau_{had}\,\tau_{had}$

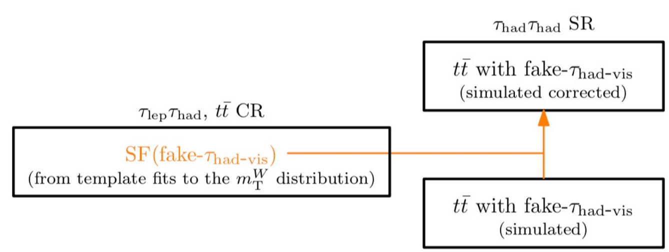

Figure 6: Schematic depiction of the fake-$\tau_{\text{had-vis}}$ scale-factor method to estimate $t\bar{t}$ background with fake-$\tau_{\text{had-vis}}$ in the $\tau_{\text{had}}\tau_{\text{had}}$ channel.

$HH \to b\bar{b}\tau\tau$

- Systematic uncertainties

Table 4: Breakdown of the relative contributions to the uncertainty in the extracted signal yield divided by the MC prediction, as determined in the likelihood fit to data. These are obtained from fixing the relevant nuisance parameters in the likelihood fit, and subtracting the obtained uncertainty on the fitted signal yield divided by the MC prediction in quadrature from the total uncertainty, and then dividing the result by the total uncertainty. The sum in quadrature of the individual components differs from the total uncertainty due to correlations between the groups of uncertainties.

Uncertainty source	Non-resonant HH	Resonant $X \to HH$ 300 GeV	Resonant $X \to HH$ 500 GeV	Resonant $X \to HH$ 1000 GeV
Data statistical	83%	75%	89%	88%
Systematic	56%	66%	45%	48%
Experimental				
Jet and $E_{\mathrm{T}}^{\mathrm{miss}}$	7%	28%	5%	4%
b-jet tagging	3%	6%	3%	3%
$\tau_{\mathrm{had\text{-}vis}}$	6%	13%	3%	7%
Electrons and muons	3%	3%	2%	1%
Luminosity & Pileup	3%	2%	2%	5%
$t\bar{t}$ and Z + HF normalisations	6%	11%	5%	3%
Theoretical and Modelling				
Fake-$\tau_{\mathrm{had\text{-}vis}}$	10%	22%	7%	7%
Top-quark	25%	21%	13%	8%
$Z(\to \tau\tau)$ + HF	10%	22%	10%	15%
Single Higgs boson	30%	2%	15%	14%
Other background	3%	2%	6%	2%
Signal modelling	7%	15%	13%	34%
MC statistical	29%	44%	33%	18%

Resonant $HH \rightarrow b\bar{b}\tau\tau$ results

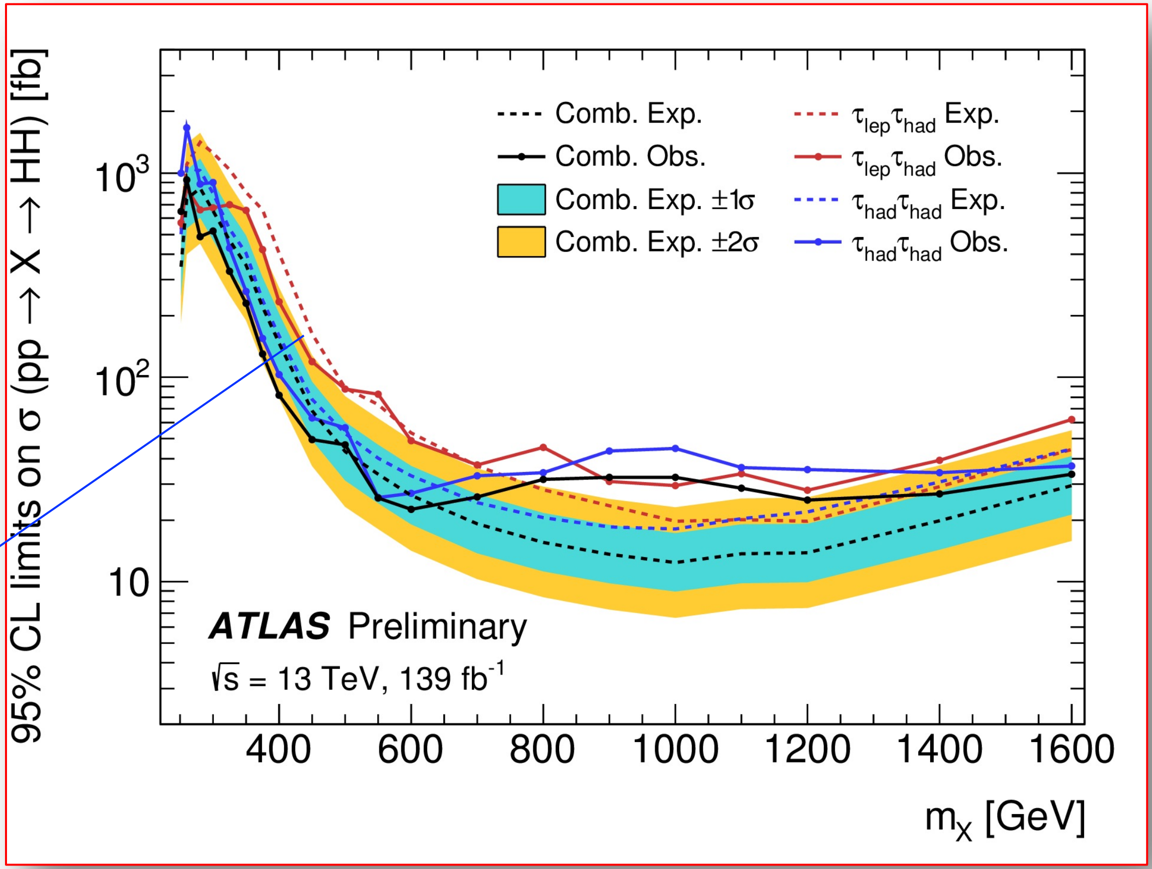

$\tau_{had}\,\tau_{had}$

Better sensitivity below 1 TeV

Statistically dominated, largest sys from signal and background modeling

- Broad excess @ 700 GeV < *m*X < 1.2 TeV.
- Most significant excess for $\tau_{had}\,\tau_{had}$ ($\tau_{lep}\,\tau_{had}$) found @ 1 TeV (1.1 TeV), local significance of 2.8 σ (1.6 σ).
- Combined: @1 TeV, local significance 3.1 σ, global significance of $2.1^{+0.4}_{-0.2}$ σ.
- Deficit @ 280 GeV with a local significance of 2.4 σ.

$HH \to b\bar{b}b\bar{b}$ analysis (1)

Largest BR, but **large multi-jet backgrounds** and challenging combinatorics

Only ggF **resonant** production considered

12 different b-jet & jet triggers for *resolved* (eff up to 80%), single jet trigger for *boosted* (eff ~80%)

Resolved
(251 GeV – 1.5 TeV)
4 b-tagged ΔR=0.4 jets

& Boosted
(900 GeV – 3 TeV)
b-tagged ΔR=1.0 and VR track-jets

Combined in the overlap region

77% btag WP
muon-in-jet+p_T-reco

Object selection

Event categorization

Resolved:
4b signal region (2b category for bkg estimate)

BDT to pair jets from Higgs
(65-100% eff)

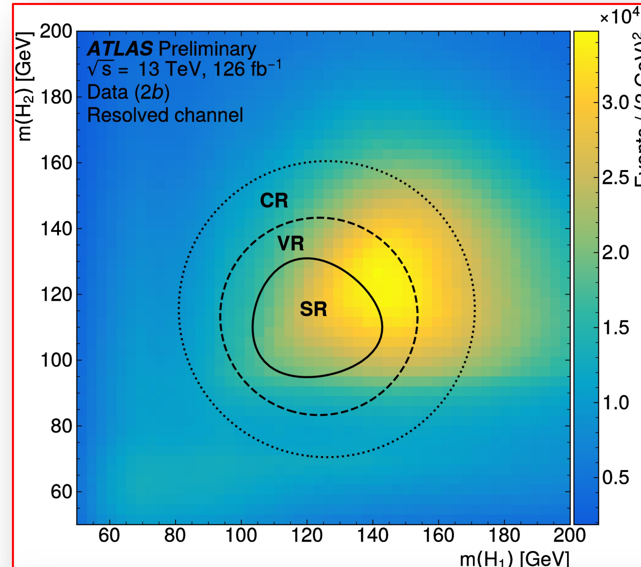

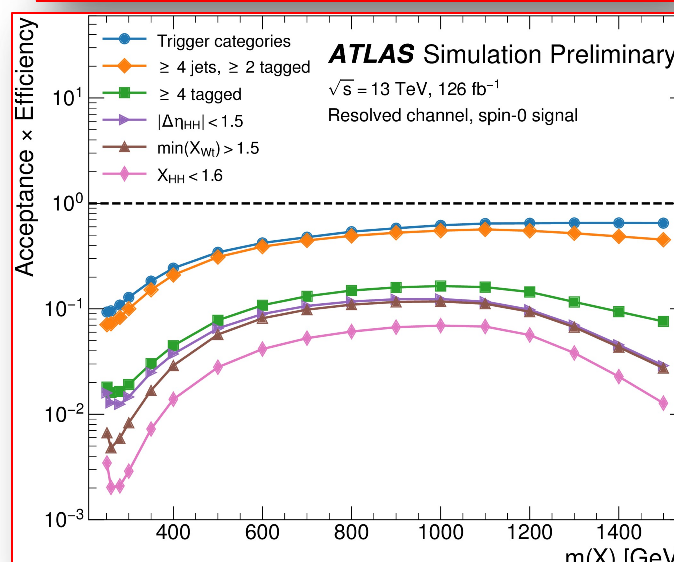

$HH \to b\bar{b}b\bar{b}$ analysis (2)

Largest BR, but **large multi-jet backgrounds** and challenging combinatorics

Only ggF **resonant** production considered

12 different b-jet & jet triggers for *resolved* (eff up to 80%), single jet trigger for *boosted* (eff ~80%)

Object selection

Resolved
(251 GeV – 1.5 TeV)
4 b-tagged ΔR=0.4 jets

& Boosted
(900 GeV – 3 TeV)
b-tagged ΔR=1.0 and VR track-jets

Combined in the overlap region

77% btag WP
muon-in-jet+p_T-reco

Event categorization

Resolved:
4b signal region (2b category for bkg estimate)

BDT to pair jets from Higgs (65-100% eff)

Background modeling

Resolved:
Bkg dominated by multi-jet + ~5% ttbar

Use 2-tag data (and apply NN-based kinematic reweighting) to derive an extrapolation from the CR into the SR.

Statistical analysis

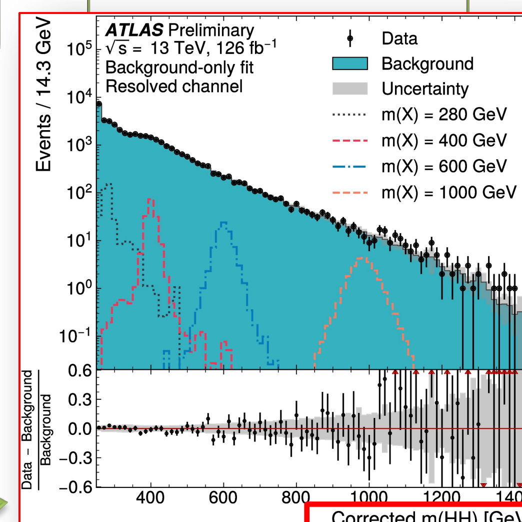

$HH \to b\bar{b}b\bar{b}$ analysis (3)

Largest BR, but **large multi-jet backgrounds** and challenging combinatorics

Only ggF **resonant** production considered

12 different b-jet & jet triggers for *resolved* (eff up to 80%), single jet trigger for *boosted* (eff ~80%)

Resolved
(251 GeV – 1.5 TeV)
4 b-tagged ΔR=0.4 jets

& Boosted
(900 GeV – 3 TeV)
b-tagged ΔR=1.0 and VR track-jets

Combined in the overlap region

77% btag WP
muon-in-jet+p_T-reco

Object selection

Event categorization

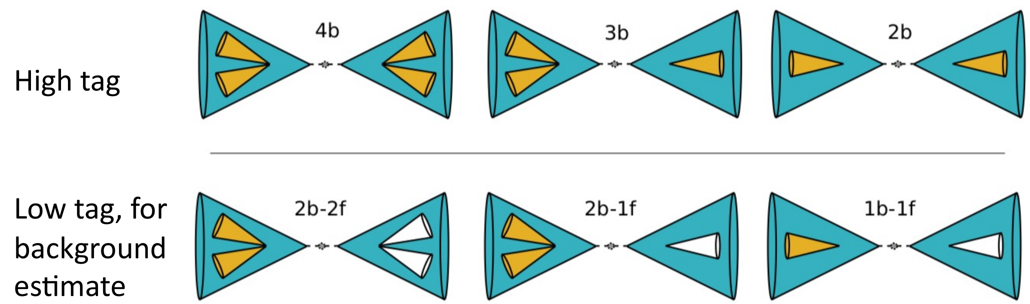

Boosted:
3 signal-enriched categories
4b, 3b, 2b

(b-tag inefficient at high p_T)

Events sorted in CR, VR & SR like in the *resolved* case

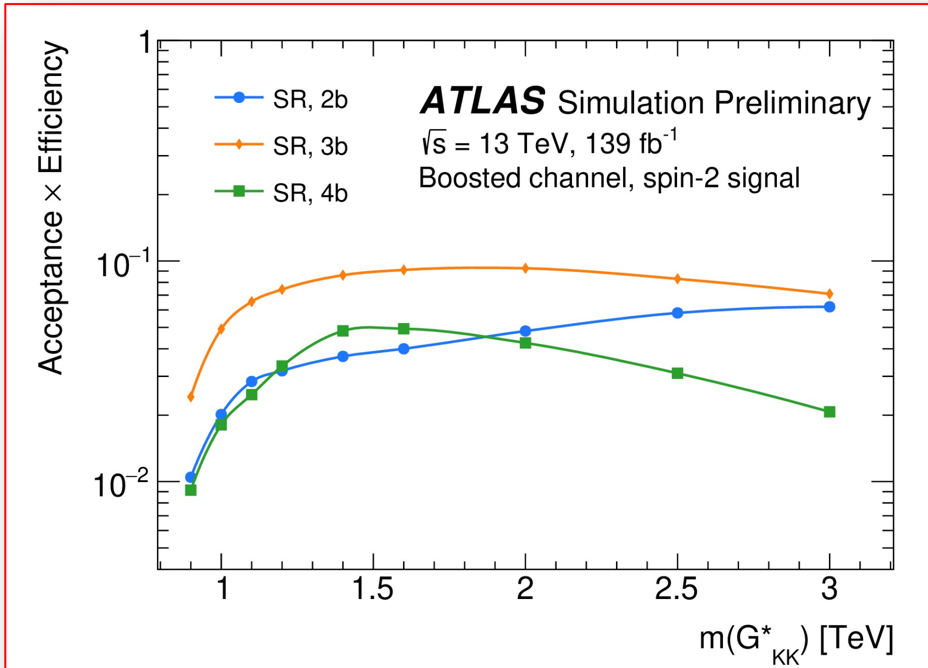

$HH \to b\bar{b}b\bar{b}$ analysis (4)

Largest BR, but **large multi-jet backgrounds** and challenging combinatorics

Only ggF **resonant** production considered

12 different b-jet & jet triggers for *resolved* (eff up to 80%), single jet trigger for *boosted* (eff ~80%)

Object selection

Resolved
(251 GeV – 1.5 TeV)
4 b-tagged ΔR=0.4 jets

& Boosted
(900 GeV – 3 TeV)
b-tagged ΔR=1.0 and VR track-jets

Combined in the overlap region

77% btag WP
muon-in-jet+p_T-reco

Event categorization

Boosted:
3 signal-enriched categories
4b, 3b, 2b

(b-tag inefficient at high p_T)

Events sorted in CR, VR & SR like in the *resolved* case

Background modeling

Boosted:
Bkg dominated by multi-jet + ~10/15/30% ttbar in the 4/3/2b regions

Data-driven MJ & MC-driven ttbar (data-driven corrections in 2/3 b)

Same reweighting approach as in the [36fb^{-1} analysis]

$$N^{n_b}_{i,\text{data}} = \mu^{n_b}_{\text{MJ}}(N^{n_b-1f}_{i,\text{data}} - N^{n_b-1f}_{i,t\bar{t}}) + \alpha^{n_b}_{t\bar{t}} N^{n_b}_{i,t\bar{t}}.$$

Statistical Analysis

(3 categories)

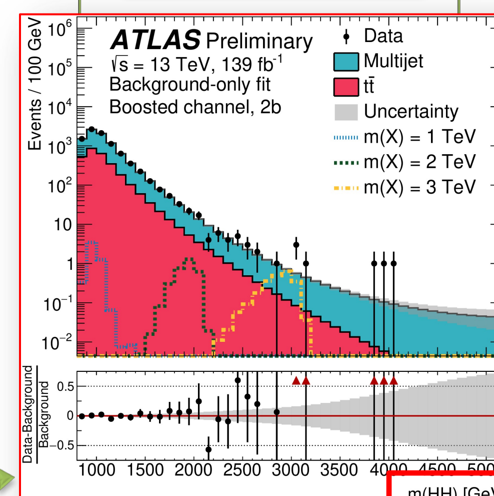

$HH \to b\bar{b}b\bar{b}$ analysis resolved

$$R_{HH}^{\mathrm{VR}} \equiv \sqrt{\left(m(H_1) - 1.03 \times 120\,\mathrm{GeV}\right)^2 + \left(m(H_2) - 1.03 \times 110\,\mathrm{GeV}\right)^2} < 30\,\mathrm{GeV}.$$

Finally, the *control region* (CR) contains the events not in the SR or VR which satisfy the condition

$$R_{HH}^{\mathrm{CR}} \equiv \sqrt{\left(m(H_1) - 1.05 \times 120\,\mathrm{GeV}\right)^2 + \left(m(H_2) - 1.05 \times 110\,\mathrm{GeV}\right)^2} < 45\,\mathrm{GeV}.$$

The centers of the VR and CR are shifted with respect to the SR to ensure that the mean H candidate masses are equal in the three regions. The shapes of these regions in the $m(H_1)$–$m(H_2)$ plane are shown with the $2b$ data in Figure 2.

After the full selection, the final discriminating variable "corrected $m(HH)$" is constructed. This is obtained by rescaling the four-momenta of the H candidates such that $m(H_1) = m(H_2) = 125\,\mathrm{GeV}$. The corrected $m(HH)$ is then the invariant mass of the sum of the two resulting four-momenta. This procedure improves the scale and resolution of the reconstructed signal mass distribution by correcting for detector effects and physical processes such as radiative emission outside the jet cones. This correction improves the signal mass resolution by up to 25% and shifts the mean of the mass distribution closer to the true value, but has a negligible effect on the background. The signal efficiency times acceptance for the various event selection steps is shown in Figure 3. The efficiency at low resonance masses is mainly limited by the trigger. At high resonance masses the jets start to merge together and the reconstruction and b-tagging efficiencies decrease. The efficiency is substantially larger for the spin-2 model than for the spin-0 model because the corrected $m(HH)$ distribution of the spin-2 model is much broader, particularly on the high-mass side.

$HH \to b\bar{b}b\bar{b}$ analysis resolved: kinematic reweighting

$$w(\vec{x}) = \frac{p_{4b}(\vec{x})}{p_{2b}(\vec{x})},$$

where $p_{2b}(x)$ and $p_{4b}(x)$ are the probability density functions for $2b$ and $4b$ data, respectively, over a set of kinematic variables x.

The computation of $w(\vec{x})$ is a density ratio estimation problem, for which a variety of approaches exist. The method employed in this analysis is modified from Refs. [77, 78] and makes use of an artificial neural network (NN). This NN is trained on $2b$ and $4b$ CR data to minimize the loss function:

$$\mathcal{L}(w(\vec{x})) = \int d\vec{x} \left[\sqrt{w(\vec{x})} p_{2b}(\vec{x}) + \frac{1}{\sqrt{w(\vec{x})}} p_{4b}(\vec{x}) \right]. \tag{6}$$

$HH \to b\bar{b}b\bar{b}$ analysis resolved: kinematic reweighting

The kinematic variables used to make up *x* are chosen to be sensitive to the differences between the 2*b* and 4*b*

1. $\log(p_T)$ of the selected jet with the 2^{nd}-highest p_T,
2. $\log(p_T)$ of the selected jet with the 4^{th}-highest p_T,
3. $\log(\Delta R)$ between the two selected jets with the smallest ΔR,
4. $\log(\Delta R)$ between the other two selected jets,
5. the average $|\eta|$ of selected jets,
6. $\log(p_T)$ of the HH system,
7. ΔR between the two H candidates,
8. $\Delta\phi$ between the jets making up H_1,
9. $\Delta\phi$ between the jets making up H_2,
10. $\log(\min(X_{Wt}))$, and
11. the number of jets in the event with $p_T > 40$ GeV and $|\eta| < 2.5$, including jets that are not selected.

There are two main sources of uncertainties: uncertainties from finite statistics in the CR, and physical differences between the CR and SR.

$HH \to b\bar{b}b\bar{b}$ analysis

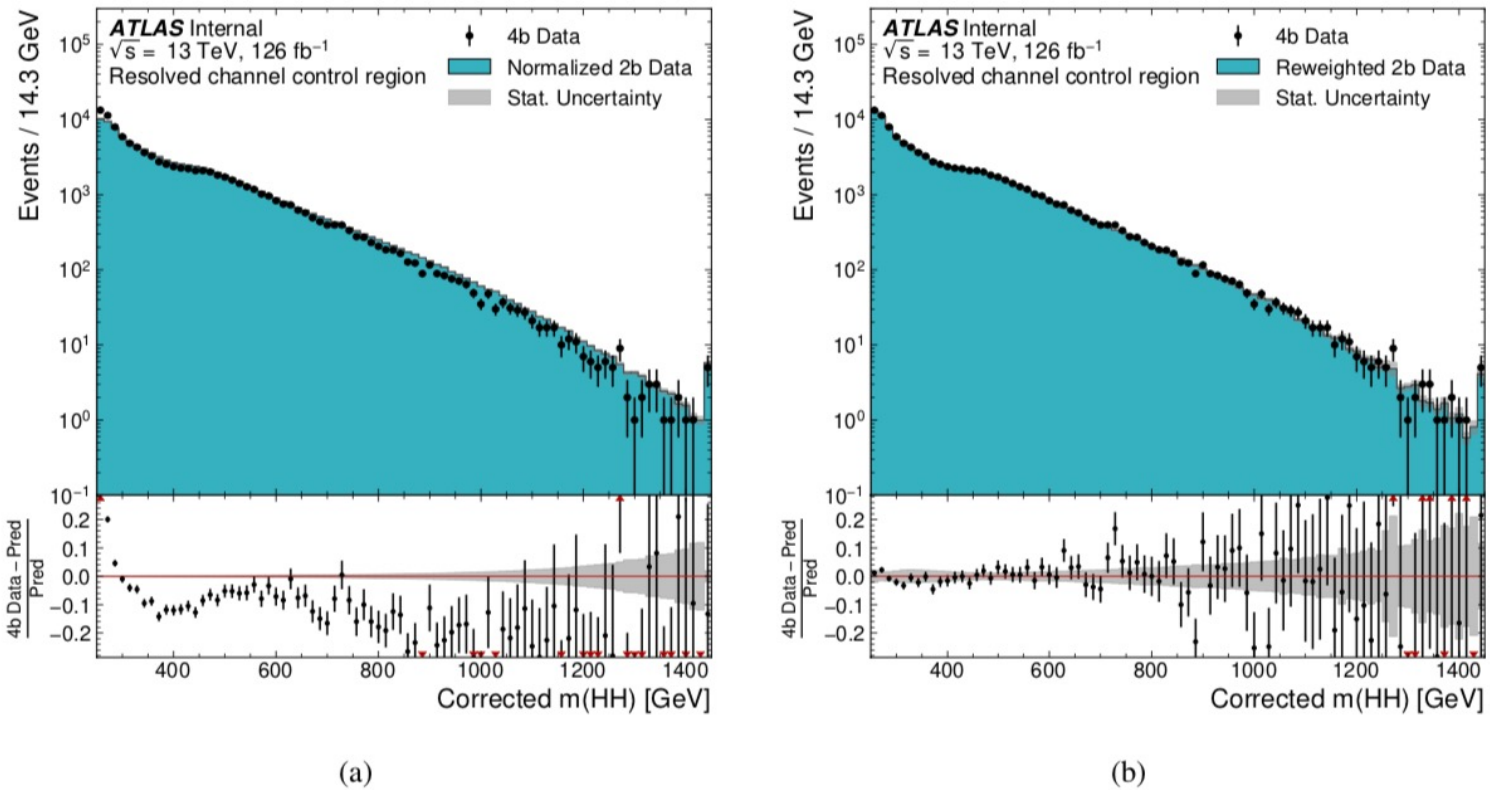

Figure 4: Corrected $m(HH)$ distributions for the $2b$ control region (teal histogram) and $4b$ control region (dots) in the resolved channel. The statistical uncertainty in the $2b$ control region is represented by the grey band. The error bars on the $4b$ points represent the Poisson uncertainties corresponding to their event yields. The $2b$ data are shown (a) before and (b) after the kinematic reweighting procedure. In both cases the $2b$ distributions are normalized to the $4b$ event yields for a pure shape comparison. The final bin of each distribution includes overflow. The bottom panel shows the difference between the $4b$ and $2b$ distributions, normalized to the $4b$ distribution.

$HH \rightarrow b\bar{b}b\bar{b}$ analysis

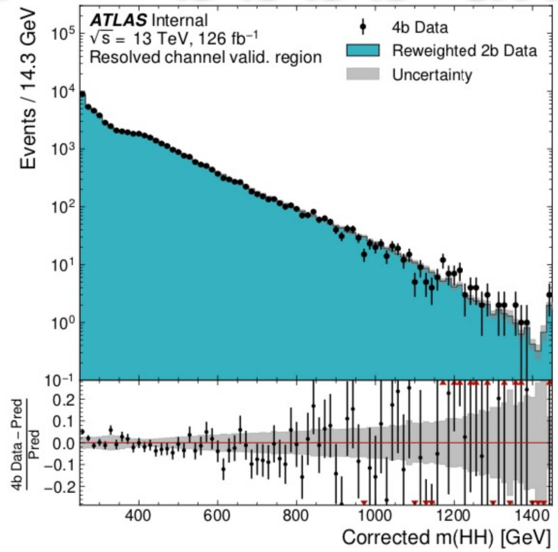

Table 1: Resolved $4b$ signal region data, estimated background, and signal event yields in corrected $m(HH)$ windows containing roughly 90% of each signal, for representative spin-0 mass hypotheses. The signal is normalized to the overall expected limit on its cross-section; its uncertainties are evaluated by adding all individual components in quadrature and are treated as correlated across corrected $m(HH)$ bins. The background yields and uncertainties are evaluated after a background-only fit to the data.

$m(X)$ [GeV]	Corrected $m(HH)$ range [GeV]	Data	Background model	Spin-0 signal model
260	[250, 321)	18 554	18 300 ± 110	503 ± 43
500	[464, 536)	2 827	2 866 ± 22	105.4 ± 5.7
800	[750, 850)	358	366.2 ± 7.3	37.7 ± 1.7
1200	[1079, 1250)	68	52.6 ± 1.7	11.71 ± 0.62

Table 2: Resolved $4b$ signal region data, estimated background, and signal event yields in corrected $m(HH)$ windows containing roughly 90% of each signal, for representative spin-2 mass hypotheses. The signal is normalized to the overall expected limit on its cross-section; its uncertainties are evaluated by adding all individual components in quadrature and are treated as correlated across corrected $m(HH)$ bins. The background yields and uncertainties are evaluated after a background-only fit to the data.

$m(G^*_{\mathrm{KK}})$ [GeV]	Corrected $m(HH)$ range [GeV]	Data	Background model	Spin-2 signal model
260	[250, 393)	26 775	26 650 ± 130	368 ± 25
500	[464, 636)	4 655	4 719 ± 37	138.6 ± 5.7
800	[707, 950)	795	811 ± 13	52.1 ± 1.9
1200	[993, 1279)	146	120.6 ± 2.8	14.45 ± 0.67

$HH \rightarrow b\bar{b}b\bar{b}$ analysis boosted

background distribution. The VR contains the events not in the SR which satisfy the condition

$$R_{HH}^{\mathrm{VR}} \equiv \sqrt{\left(m(H_1) - 124\,\mathrm{GeV}\right)^2 + \left(m(H_2) - 115\,\mathrm{GeV}\right)^2} < 33\,\mathrm{GeV}. \tag{9}$$

Finally, the CR contains the events not in the SR or VR which satisfy the condition

$$R_{HH}^{\mathrm{CR}} \equiv \sqrt{\left(m(H_1) - 134\,\mathrm{GeV}\right)^2 + \left(m(H_2) - 125\,\mathrm{GeV}\right)^2} < 58\,\mathrm{GeV}. \tag{10}$$

The CR is shifted to higher masses relative to the signal and validation regions in order to maximize statistics while avoiding the low-mass peak of the multijet background distribution. The definition of these regions in the $m(H_1) - m(H_2)$ plane are shown with the $2b$-$1f$ data in Figure 8.

In order to ensure orthogonality between the resolved and boosted channels, any events passing the resolved signal region selection are vetoed from the boosted channel. This priority choice results in the best signal sensitivity.

$HH \to b\bar{b}b\bar{b}$ analysis boosted

The sizes of the multijet and $t\bar{t}$ estimates are obtained from a normalization fit to the CR data in each category. Two normalization parameters μ_{MJ} and $\alpha_{t\bar{t}}$ per b-tagging category are introduced as follows:

$$N_{i,\mathrm{data}}^{n_b} = \mu_{\mathrm{MJ}}^{n_b}(N_{i,\mathrm{data}}^{n_b-1f} - N_{i,t\bar{t}}^{n_b-1f}) + \alpha_{t\bar{t}}^{n_b} N_{i,t\bar{t}}^{n_b}. \quad (11)$$

Table 3: Best-fit values for μ_{MJ} and $\alpha_{t\bar{t}}$, with statistical uncertainties on the parameters. The linear correlation coefficient between both parameters is also given. The value of $\alpha_{t\bar{t}}$ in the $4b$ region is fixed to 1, since the data are unable to constrain it significantly.

Region	$2b$	$3b$	$4b$
μ_{MJ}	0.05428 ± 0.00057	0.1201 ± 0.0024	0.0269 ± 0.0015
$\alpha_{t\bar{t}}$	0.827 ± 0.011	0.771 ± 0.041	1
Correlation	-0.74	-0.74	0

For $3b$ and $2b$, a kinematic reweighting procedure is applied to each corresponding low-tag category, analogous to the resolved channel. For the $4b$ category, no kinematic reweighting is applied. This is because the effect of mismodelings due to b-tagging is small compared to the size of statistical uncertainties in this category. Instead of an NN for constructing the reweighting function, an iterative spline method based on the one used in Ref. [8] is implemented here.

$HH \rightarrow b\bar{b}b\bar{b}$ analysis boosted

The difference between these low-tag and high-tag regions is that the low-tag events have an untagged H candidate (0 b-tagged track jets), while high-tag events instead have a tagged H candidate (exactly 1 b-tagged track jet, since only the $3b$ and $2b$ categories are considered here). Therefore, the reweighting is applied to low-tag events based on their untagged H candidates, with the aim to match the kinematics of the tagged H candidates in high-tag events. This reweighting is derived purely in the low-tag regions; the tagged H candidates in the $1b$-$1f$ category are used to define the target.

The following kinematic distributions are used to construct the reweighting, for which leading and subleading refer to an ordering in p_{T}:

1. p_{T} of the H candidate,
2. p_{T} of the chosen track jet,
3. η of the chosen track jet, and
4. ΔR between the leading and subleading track jets (for H candidates with at least two track jets).

$HH \to b\bar{b}b\bar{b}$ analysis boosted

The "chosen" track jet is the b-tagged one for tagged H candidates and a random one for untagged H candidates. In tagged H candidates with two track jets, the leading and subleading track jets have roughly equal probabilities to be the b-tagged one, so this random selection does not introduce significant bias. Separate distributions are constructed for leading and subleading H candidates, as well as for leading and subleading track jets.

At each iteration i, cubic splines are fit to the ratios of tagged to untagged distributions, and the weights are updated according to

$$w_i(\vec{x}) = w_{i-1}(\vec{x}) \times \left[\left(\prod_j f_{ij}(x_j) - 1 \right) \times r_i + 1 \right], \qquad (12)$$

$HH \to b\bar{b}b\bar{b}$ analysis systematics

Table 6: Impacts of the main systematic uncertainties on the expected 95% CL upper limits on the signal cross-section times branching ratio. These are defined as the relative decrease in the expected limit when each relevant nuisance parameter is held fixed to its best-fit value instead of being assigned an uncertainty. The spin-0 signal model is used here.

Uncertainty category	Relative impact (%)		
	280 GeV	600 GeV	1600 GeV
Background $m(HH)$ shape	12	8.7	1.3
Jet momentum/mass scale	0.6	0.1	1.5
Jet momentum/mass resolution	2.1	1.5	7.4
b-tagging calibration	0.7	0.4	1.8
Theory (signal)	0.6	0.6	1.6
Theory ($t\bar{t}$ background)	N/A	N/A	0.7
All systematic uncertainties	16	11	13

$HH \to b\bar{b}b\bar{b}$ analysis

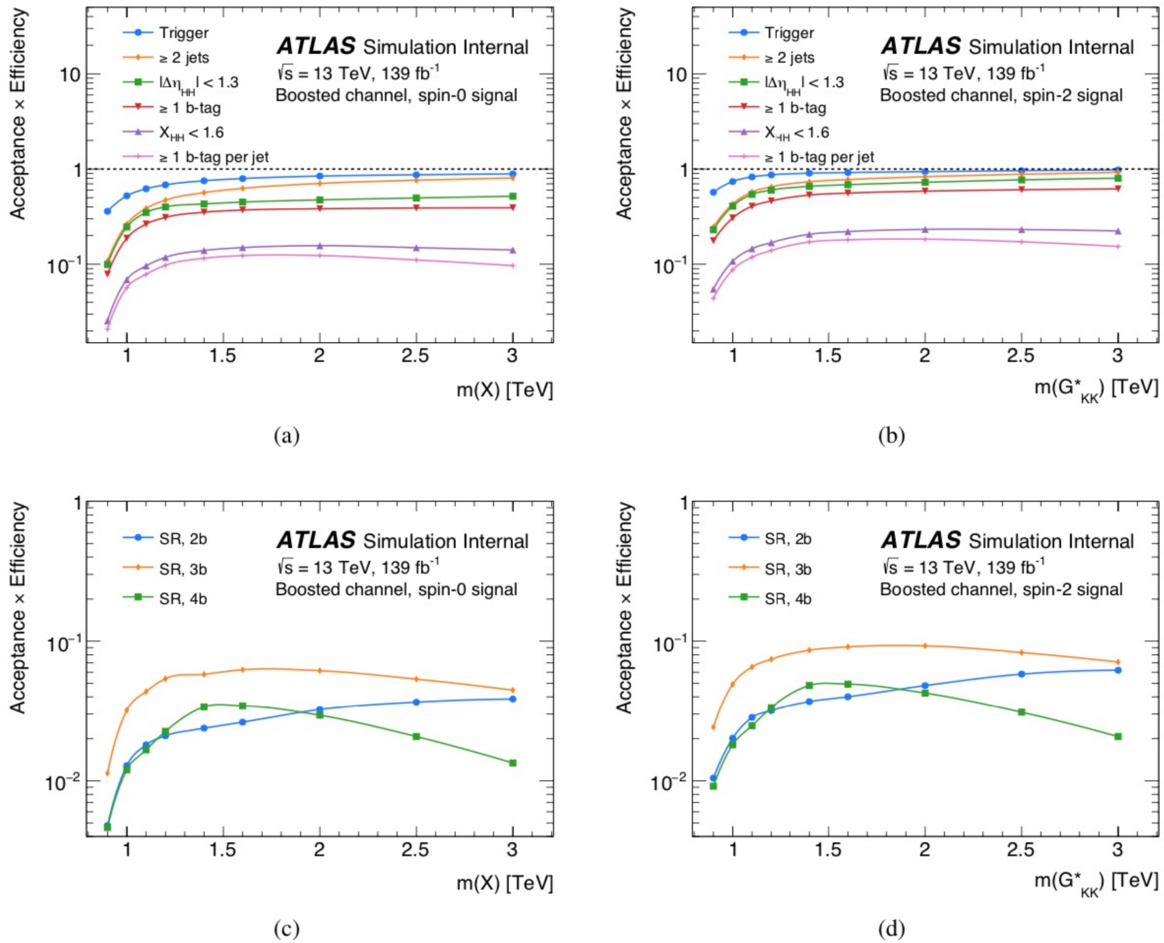

(a) (b)

(c) (d)

Figure 9: Cumulative signal acceptance times efficiency as a function of the resonance mass for various selection steps in the boosted channel. The steps up to the b-tag categorization are shown for (a) the spin-0 and (b) the spin-2 signal models. The efficiencies of the three b-tag categories are shown for (c) the spin-0 and (d) the spin-2 scenarios; this efficiency is obtained after the other selection steps including the SR definition. The signal efficiency in the $4b$ region has a maximum around 1.5 TeV. Above that value the track jets starts to merge together, and for the highest resonance masses the $2b$ category becomes the most efficient.

VBF 4b

https://link.springer.com/article/10.1007/JHEP07(2020)108

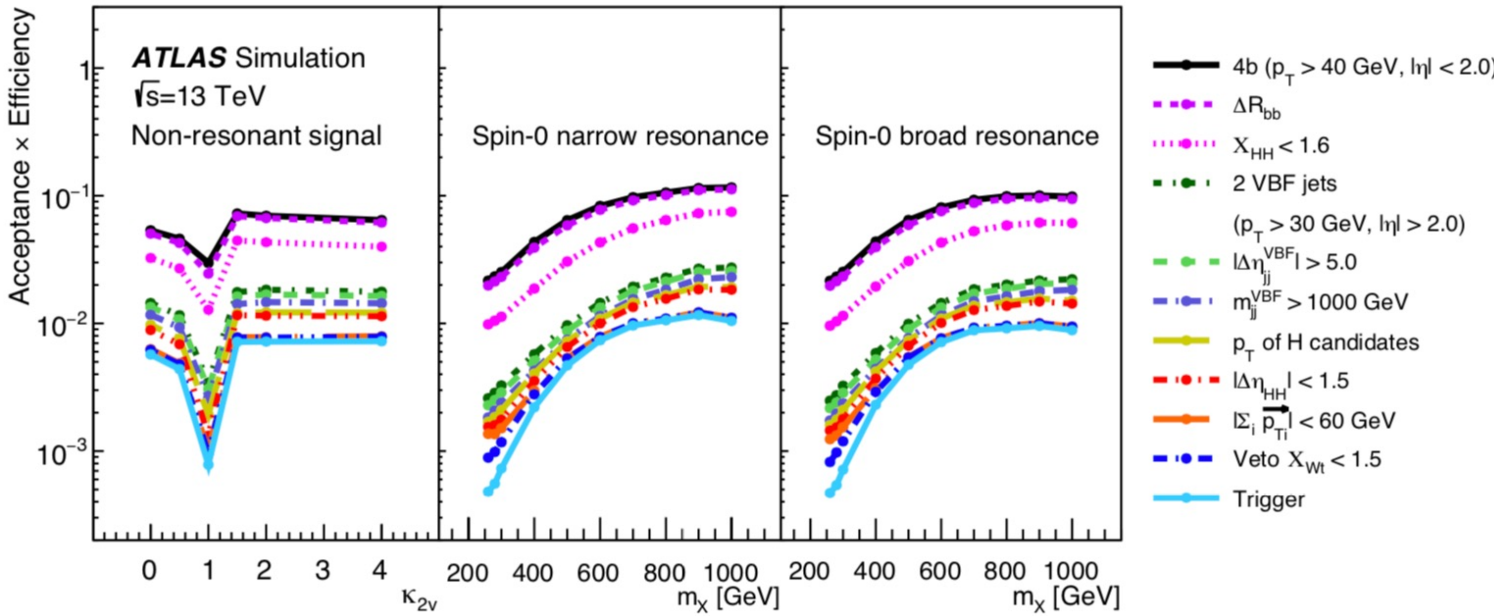

Figure 2: Cumulative acceptance times efficiency at each stage of the event selection, as detailed in Section 5. The number of events surviving the selection divided by the number of generated events is reported separately for the non-resonant signal as a function of the κ_{2V} coupling modifier and for the narrow- and broad-width resonance production hypotheses as a function of the generated mass.

VBF 4b

https://link.springer.com/article/10.1007/JHEP07(2020)108

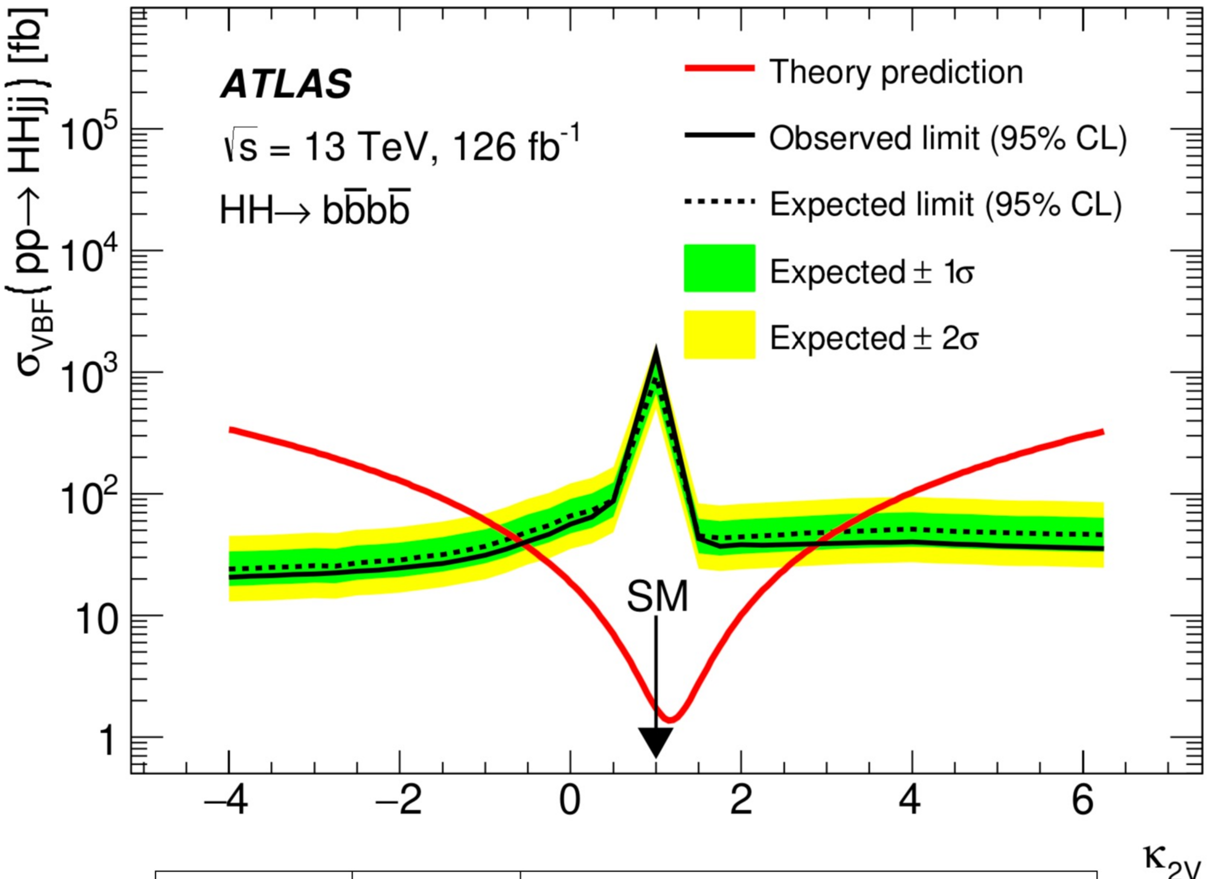

	Observed	-2σ	-1σ	Expected	$+1\sigma$	$+2\sigma$
σ_{VBF} [fb]	1450	500	660	920	1280	1720
$\sigma_{\mathrm{VBF}}/\sigma_{\mathrm{VBF}}^{\mathrm{SM}}$	840	290	390	540	750	1000

Di-Higgs Combination

Early Run 2 results

Non-resonant ggF production

ATLAS

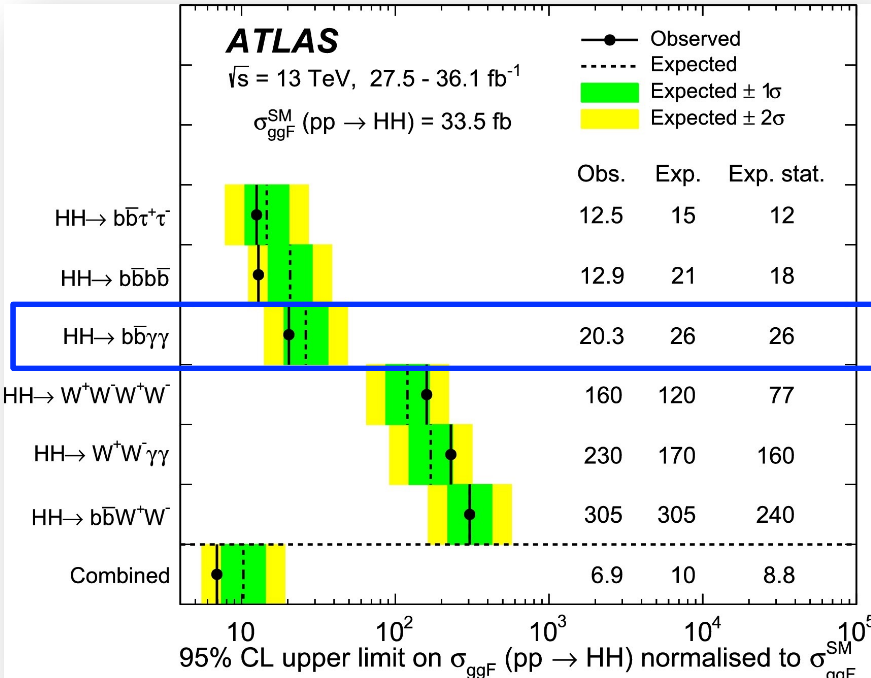

CMS

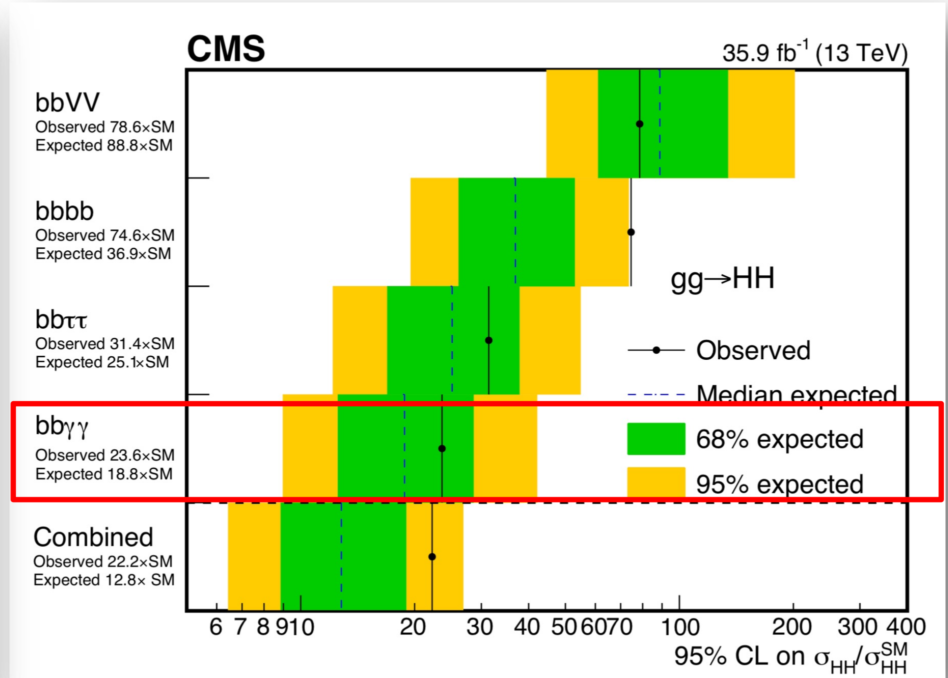

Different ATLAS-CMS "ranking" for the 3 most sensitive channels

Differences in analysis strategy lead to large differences in sensitivity and final results…

Early Run 2 Results

https://www.sciencedirect.com/science/article/pii/S0370269319308251?via%3Dihub#fg0050

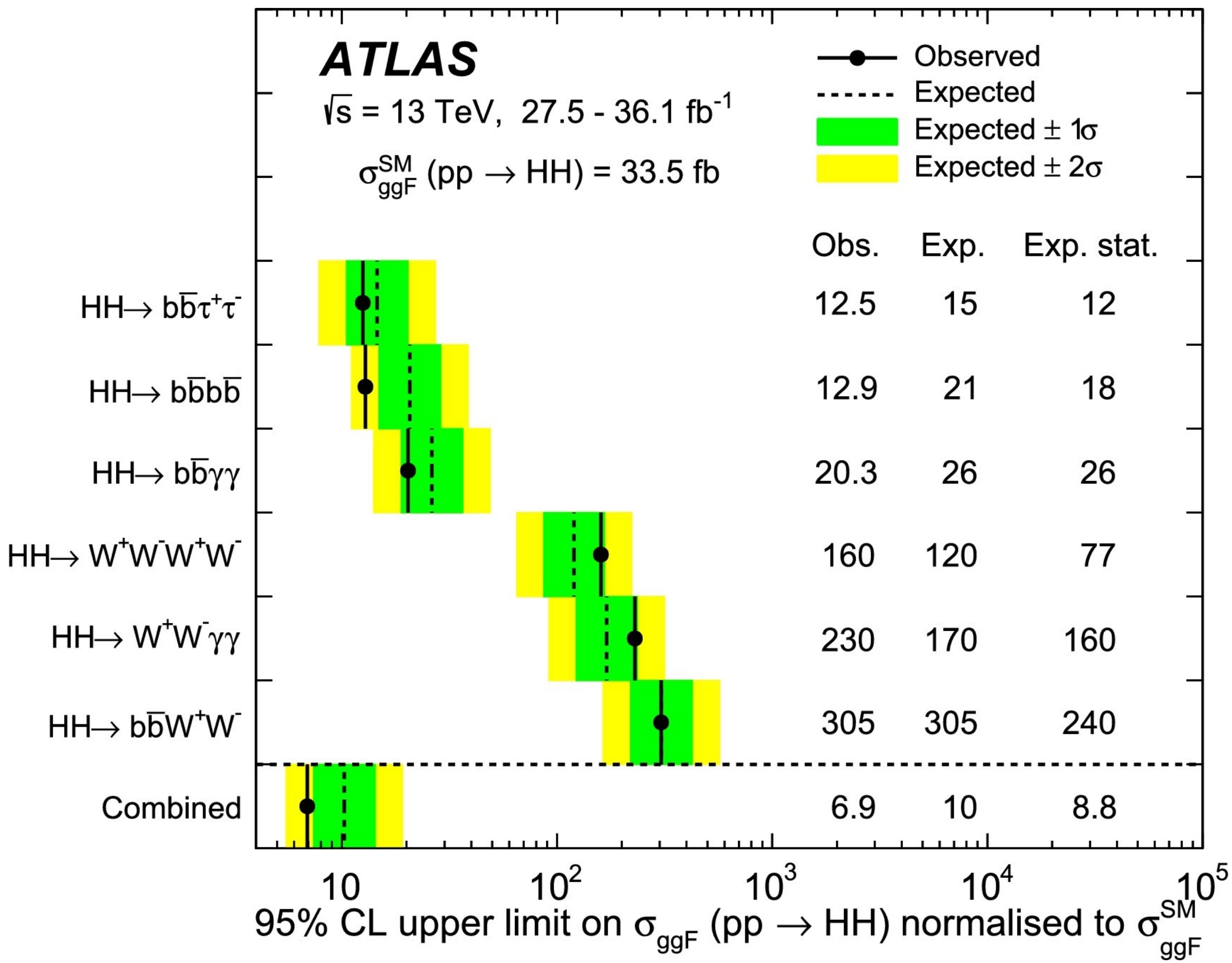

Early Run 2 Results

https://www.sciencedirect.com/science/article/pii/S0370269319308251?via%3Dihub#fg0050

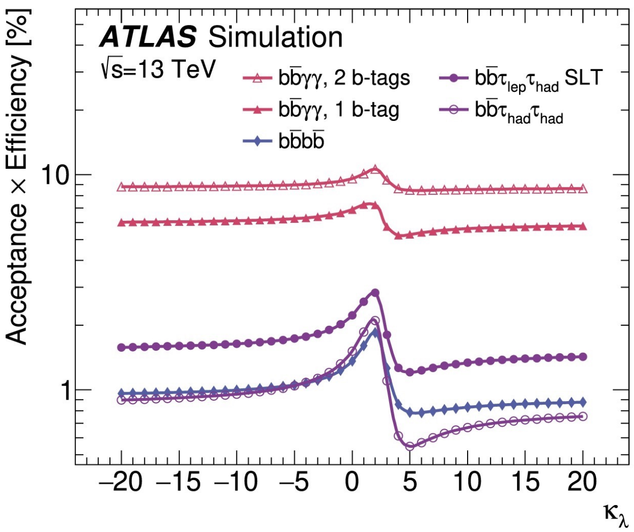

(a)

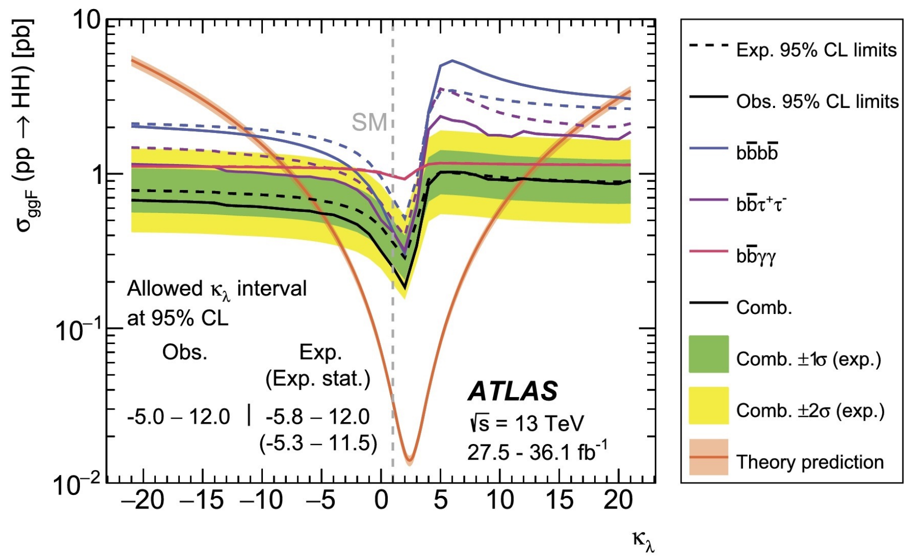

(b)

Final state	**Allowed κ_λ interval at 95% CL**		
	Obs.	**Exp.**	**Exp. stat.**
$b\bar{b}b\bar{b}$	−10.9 — 20.1	−11.6 — 18.8	−9.8 — 16.3
$b\bar{b}\tau^+\tau^-$	−7.4 — 15.7	−8.9 — 16.8	−7.8 — 15.5
$b\bar{b}\gamma\gamma$	−8.1 — 13.1	−8.1 — 13.1	−7.9 — 12.9
Combination	−5.0 — 12.0	−5.8 — 12.0	−5.3 — 11.5

Early Run 2 Results

https://www.sciencedirect.com/science/article/pii/S0370269319308251?via%3Dihub#fg0050

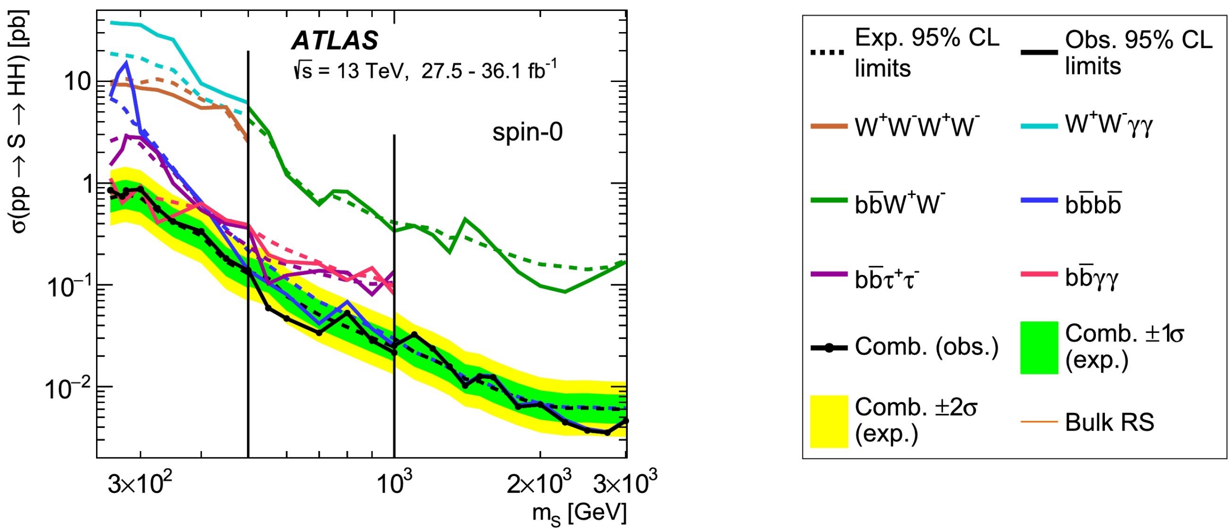

(a)

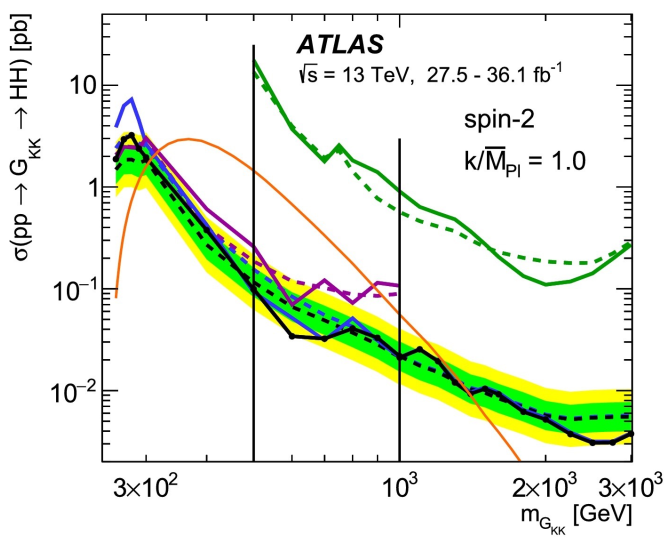

(b)

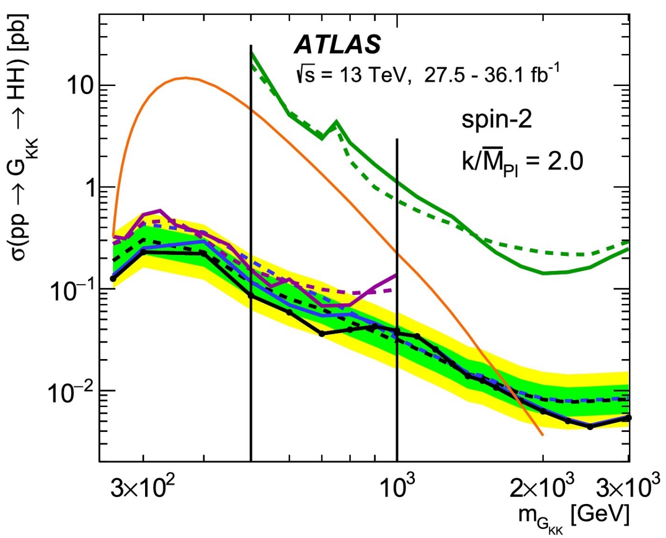

(c)